## B.15 "Predicting Failures Which Have Not Yet Been Observed — Microprocess Sequence Approach (MPSA)," by Roger W. Staehle

### 1. Background

The purpose of this background paper is to describe a conceptual approach to predicting corrosion failures that have not yet been observed but could occur after long times, such as those associated with LWRs that are re-licensed. This approach is in the category of "*proactive*" prediction, where possibly future failures are intentionally sought out, and the credibility for producing failures is assessed. This approach also challenges conventional assumptions about the cause and nature of corrosion failures. In the past, failures have occurred first; and the nuclear materials community, then, has responded usually with excellent work aimed at explaining the observations. This is "*reactive*" research. We are concerned here, rather, with the mechanics of "*proactive*" prediction.

This discussion deals with predicting corrosion processes in LWRs, although the approaches described here would apply broadly to other industries. This discussion is also mainly concerned with stress corrosion cracking (SCC) and corrosion fatigue (CF), as they are connected; and, some aspects of flow-assisted corrosion (FAC) are included. These are the most likely modes of corrosion to produce failures. Other topics of damage include wear of steam generator tubes at anti-vibration bars (AVB), but these are not discussed here, although such modes are within the scope of this approach. As discussed in this paper, failure means the initiation of degradation, its progression, eventual propagation through the component wall, or any combinations of these.

An essential assumption of this discussion is that very long times until failure are not related to a monotonic progression of SCC processes. Rather, the long times are most likely associated with other factors that produce specific local conditions that "open the gate" for SCC or other relatively rapid processes as compared to general corrosion. These preliminary processes occur over a "precursor period." Schematically, such cases are shown in Figure B.15.1. Case I corresponds to SCC, starting upon initial exposure to an environmental condition that produces SCC, as described in Section 2.1; Case I corresponds to failure processes (e.g. to LPSCC) that initiate as soon as the surfaces are exposed to primary water at operating temperature. Case II corresponds to SCC that starts after necessary conditions for initiation are achieved in relatively short times (e.g. half to 20 years), for which there are already examples as described in Section 2.2.

The approach described here for predicting failures, which have not yet occurred, is the "Microprocess Sequence Approach" (MPSA). This approach utilizes sets of elements from the environments and materials where these elements can be identified, and quantified, and connected sequentially or in parallel, to provide a scenario leading to the initiation of failure. The overall procedure is described in Figure B.15.38.

What is actually being predicted here is not the course of the SCC itself but rather the time to arrive at the conditions for SCC to start, as shown for shorter cases in Case II and much longer times in Case III of Figure B.15.1. It is assumed here that existing correlations, (e.g. from Staehle and Gorman[1]) for the occurrence of SCC will be activated once the precursor period has produced the necessary conditions for SCC to initiate.

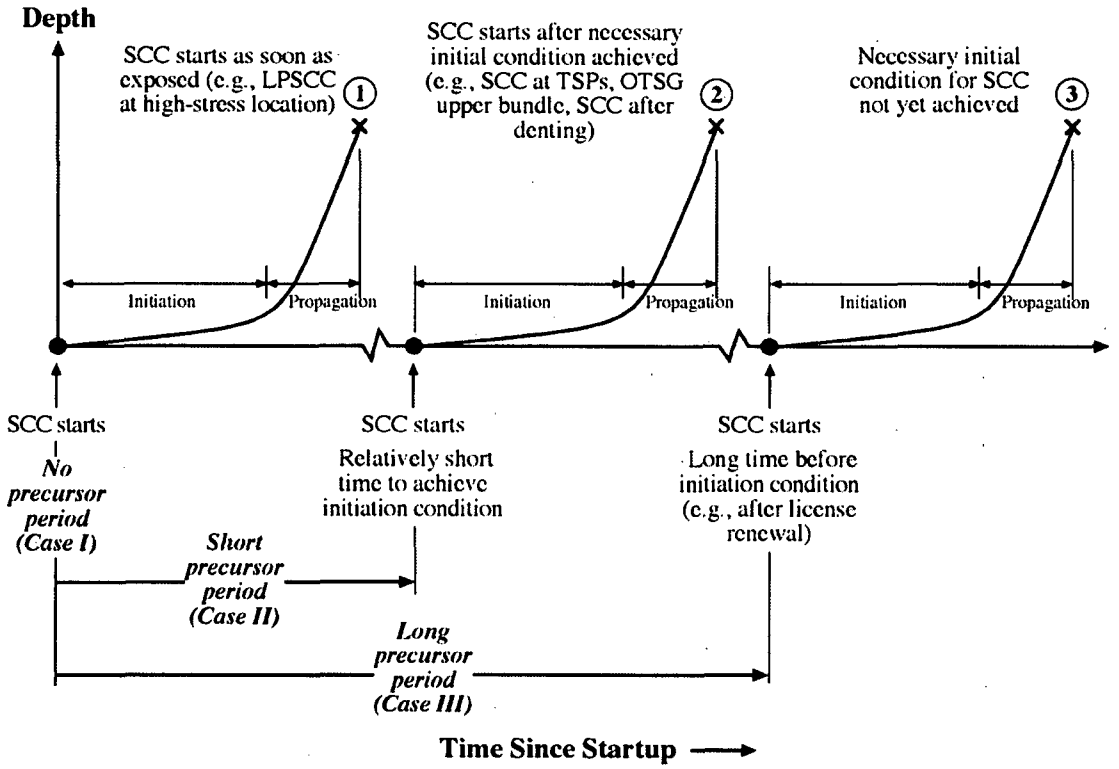


**Fig. B.15.1** Schematic view of three cases for the time-dependence of SCC. Initiation and propagation times assumed to be the same. The three cases are differentiated by the length of the precursor periods.

Such longer times should be compared with the range of time over which re-licensing is expected to occur as shown in Figure B.15.2. Relative to the schedule for re-licensing, it appears that instances of SCC in the nuclear industry have occurred in essentially three stages as suggested in Figure B.15.3. In Stage I, failures occurred in the early use of stainless steel tubes and then in Alloy 600 tubes. These failures were extensive. In Stage II, the present stage, SCC is occurring in the laboratory for Alloy 690TT and in the non-decorated grain boundaries of stainless steel. This present discussion about prediction applies to Stage III, where a proactive approach could predict occurrences of future degradation based on the reasonableness of scenarios as described in Section 5.0 and Figure B.15.38. In this Stage III, a relatively long time is consumed by the precursor period in which conditions for the occurrence of SCC must first develop before SCC can start, as shown for Case III in Figure B.15.1.

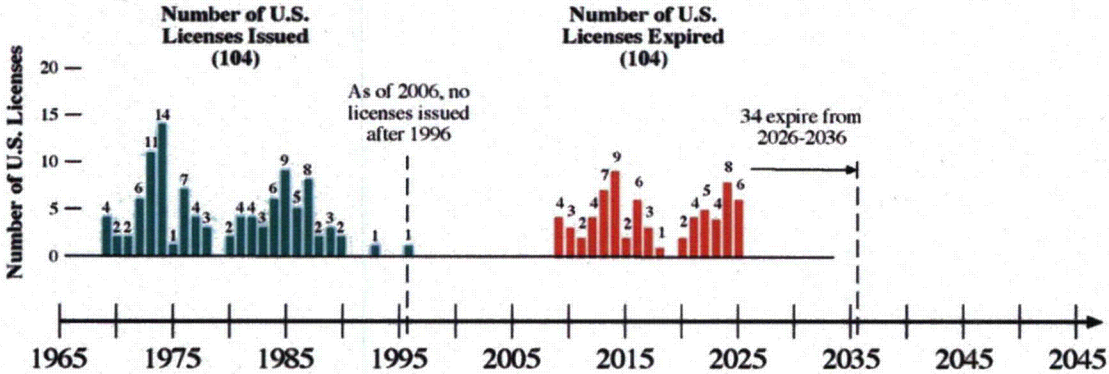


**Figure B.15.2** Number of U.S. licenses issued and expired vs. time compared with a 20-year life extension after a presumed re-licensing.

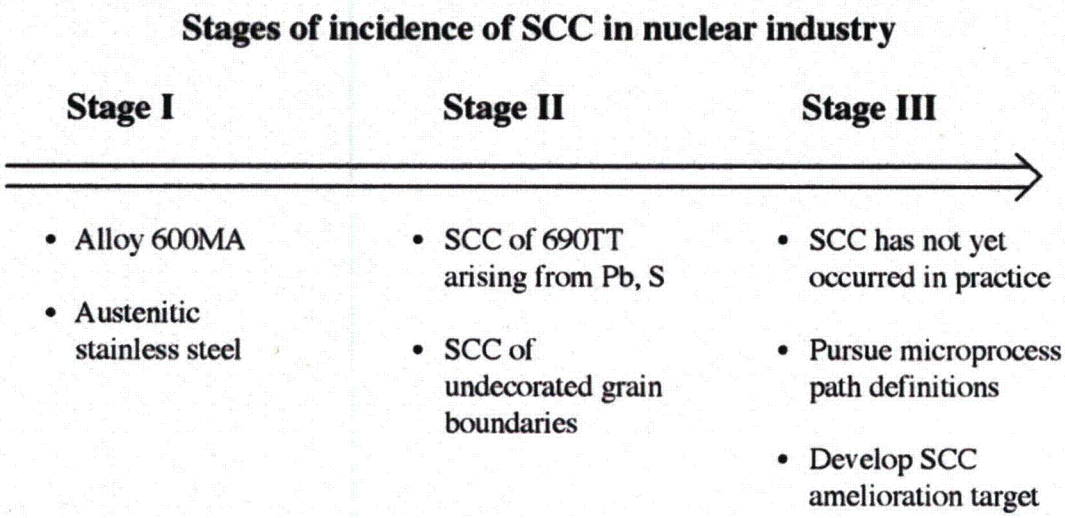


**Fig. B.15.3** Schematic illustration of the stages of SCC occurrences over time in the LWR industry.

The theme of this paper is illustrated in Figure B.15.1 for Case III. Here, the conditions that are necessary for SCC to occur have not yet fully developed during the initial licensing period. The central question, then, is: what are the processes that could produce the necessary conditions that lead to SCC at this later time? Our assertion here is that predicting SCC/CF that has not yet occurred, i.e. *proactive* prediction, can be approached credibly by using information and understandings that are already available and linking them in sensible ways to predict the time required for completion of the precursor period, of Figure B.15.1 Case III, before the SCC can start. The challenge, then, is to identify this information and explore out understandings. Such an approach is described in Sections 3.0 and 4.0.

There are, presently, no serious predictive methods for SCC that are not based on extrapolating from already existing failures. Current methods include:

- Accelerated testing and carrying forward the data, usually the mean value, with experimentally determined dependencies such as the activation energy (e.g. Q=40kcal) or the stress exponent (e.g. n=4). This is more or less how performance is predicted at the present.

- Developing correlation equations and choosing limits for scatter (e.g. three sigma) for design, i.e. safety factors.

- Enclosing scattered data with an enveloping curve and assuming that the envelope gives a conservative value.

- Taking a Bayesian statistical approach where successive failures on a cumulative distribution give progressively more confidence to the shape factor and its extrapolation.

- Using probabilistic fracture mechanics where the probability of occurrence of critically sized defects and the probabilistic evaluation of the critical stress intensity provide the basis for the probability of future failures.[2,3,4,5,6]

- Applying a "fitness for service" approach where defects are assessed at some time during service, (e.g. an inspection period), and then assessing whether these defects can lead to potential failures.

- Using the Corrosion Based Design Approach (CBDA), as described by Staehle,[7] involving the ten segments of environmental definition, material definition, mode definition, superposition, failure definition, statistical definition, accelerated testing, prediction, monitoring and inspection, and feedback.

- Using the "Locations for Analysis" ($LA_i$) approach as described by Staehle,[7] where obvious locations containing multiple stressors of relatively intense values occur together.

- Using physically based statistics for predicting the "First Failure" as described by Staehle.[8,9] Here, each of the statistical parameters is modeled using existing data for the seven primary variables as shown in Figure B.15.4. [1,9,37] The final distribution then, includes the three, now physically dependent, statistical parameters with their respective dependencies.

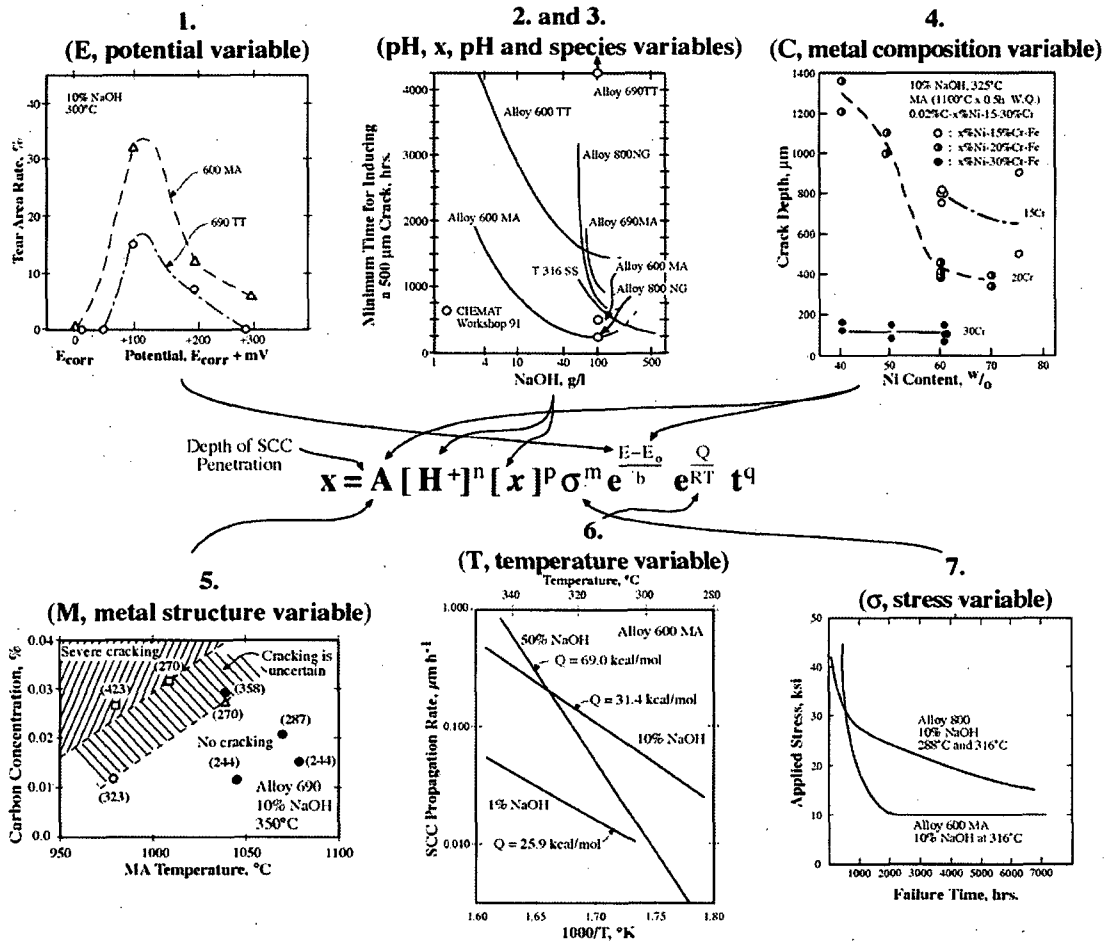


**Figure B.15.4** Examples of dependencies on the seven primary variables for SCC as they apply to a correlation equation that might be used to model the statistical parameters for a statistical distribution. These examples are taken from data, which describe SCC in alkaline solutions. These data are discussed by Staehle and Gorman.[1] © NACE International 2003/2004.

A practical question here, is how can failures that have not yet occurred be found? The essence of the approach in this paper, the "Microprocess Sequence Approach (MPSA)" for predicting the precursor conditions that must coalesce before SCC occurs, as indicated in Figure B.15.1, consists of six steps as follows:

- The influences on materials can be divided into six domains and their respective microprocesses. The breakdown of the domains is somewhat arbitrary, but practical and convenient choices are: global environment, bulk environment, outside surface, protective surface layer, inside metal surface, and bulk metal. These domains, with examples of possible microprocesses, are identified in Figure B.15.5. These domains are discussed in Sections 3.0 and 4.0.

- Identify the modes of failure of interest, (e.g. SCC, CF, FAC), and develop information bases for their dependencies of occurrence, as described in Section 6.0. These define targets for scenarios, as described in Section 5.0, which involve practical aggregations of domains and their microprocesses.

- Identify the "microprocesses" of these domains that could affect the modes of failure. These microprocesses, as they apply for the six domains, are described in Section 4.0; and examples are shown in Figure B.15.5.

- Develop likely scenarios as suggested in Figure B.15.6 and Section 5.0, which connect microprocesses of the six domains, and which have a high likelihood for leading to failure. These scenarios would constitute the precursor period as identified in Figure B.15.1 for Cases II and III.

- Quantify possibly critical microprocesses in terms of their dependence on the variables that lead to critical conditions for SCC to occur at the end of the precursor period.

- Develop critical experiments to assess whether the proposed scenarios and their component microprocesses are credible.

Predicting SCC in LWRs in the past has been hindered by overly restrictive and often poorly informed assumptions on the microprocesses such as:

- SCC occurs only in the presence of "specific ions."

- SCC does not occur either in pure environments or in pure materials; i.e. SCC of Alloy 600 in pure deoxygenated water is not credible.

- Boiling $MgCl_2$ is a suitable environment to assess the dependence of SCC on alloy composition.

- Pure water cannot produce SCC of sensitized stainless steel.

- Water chemistry used for fossil boilers should be adequate for nuclear boilers.

- Tube support crevices will not accentuate any chemistry that could lead to SCC.

- There is not sufficient Pb in feed water to produce PbSCC even if it is concentrated.

- SCC due to Pb in Alloy 600MA is transgranular.

- Stainless steel without sensitization will not sustain SCC.

- The high purity of water in secondary OTSG water will not produce deposits on superheated upper bundle surfaces.

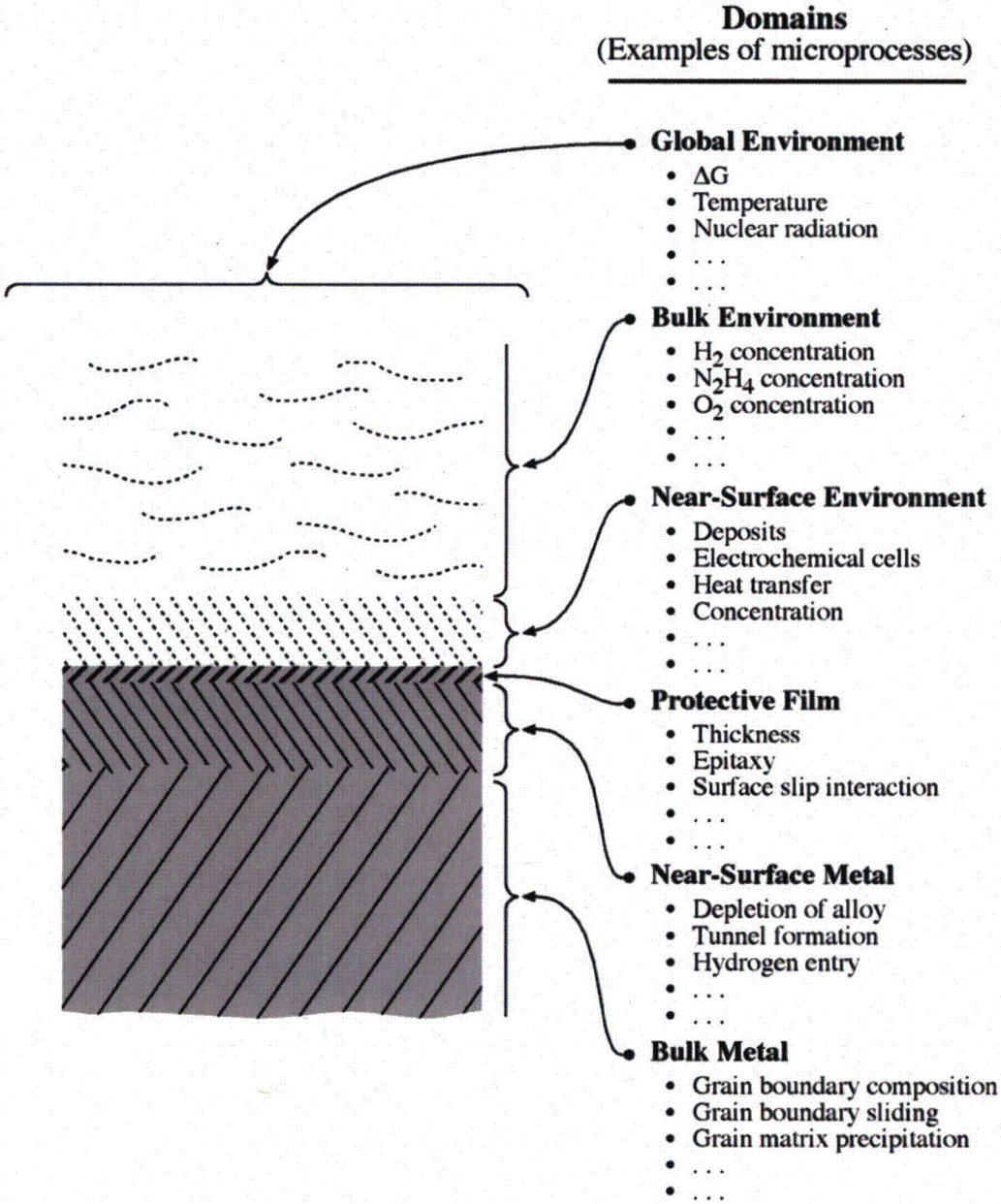


**Figure B.15.5** Schematic view of six domains for quantifying microprocesses relating to the continuum from a global environment through to the bulk metal. Examples of microprocesses indicated.

There are more such assumptions. Similar assumptions may still hinder our capacity to predict the occurrence of degradation. In Section 2.0, examples of failures, which have occurred and are already known, and which follow this microprocess route are considered and provide examples of important aspects of the MPSA approach. Section 3.0 describes domains and their inherent microprocesses; Section 4.0 describes physical details of microprocesses and their implications; Section 5.0 describes how scenarios are developed and applied; Section 6.0 describes the failure target (e.g. start of SCC after the precursor produces necessary conditions)

for the development of scenarios; finally, in Section 7.0 some predictions for future and not yet observed damage are developed based on the procedures described in this report.

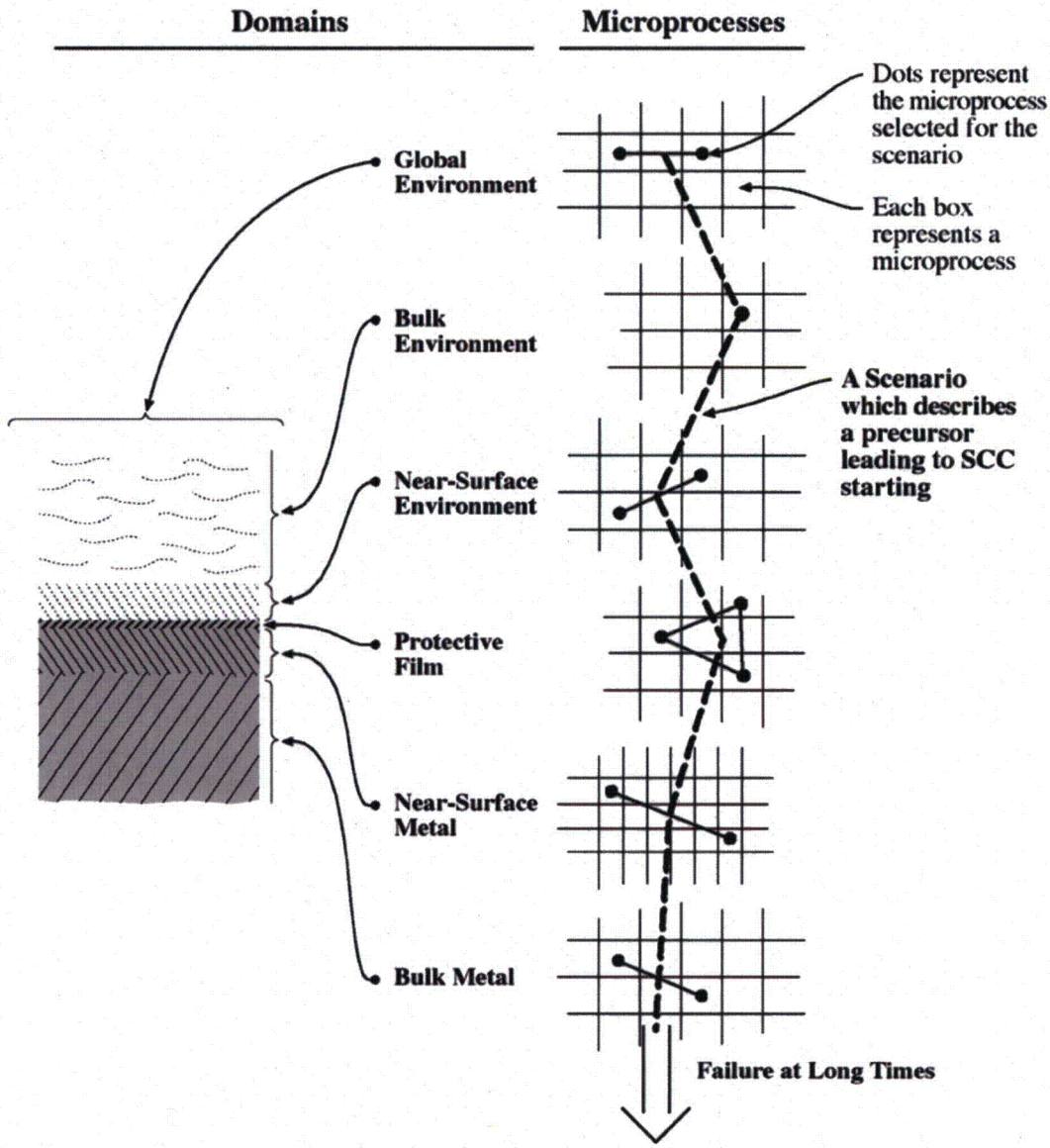


**Figure B.15.6** Schematic view of a scenario that might be developed, which links microprocesses in successive domains as the scenario would apply to the precursor stage of Figure B.15.1.

## 2. Examples of Past Sequential Failures

The purpose of this section is to describe examples of failures that correspond to Cases I and II of Figure B.15.1. These failures provide insights to how failures with longer precursor times might evolve. Section 2.1 describes failures that begin when the plant starts and where the time-to-penetration is associated with the evolution of the SCC or FAC itself with no need to develop pre-conditions over time. This corresponds to Case I of Figure B.15.1. Section 2.2 corre-

sponds to Case II of Figure B.15.1 where a relatively short (e.g. half to 20 years) precursor period precedes the evolution of the SCC itself.

## 2.1 Failures without time-dependent pre-conditions, no precursors, Case I

SCC on the primary side, LPSCC--no precursor

On the primary side of steam generator tubes there are no crevices, and the chemistry is generally constant with time. The major stressors are residual stresses and temperature; thus, any SCC that occurs does not depend on accumulation processes in a precursor period. The highest residual stresses are initially present either at small diameter U-bends or at roll transitions at the top of the tubesheet; Figure B.15.7a[10] shows data for the temperature dependence of LPSCC in the small diameter U-bends of SGs. The earliest failures at the highest temperature, about 306°C, occurred after 20-30 months. Figure B.15.7b[11] shows a cumulative distribution function (cdf) in Weibull coordinates for the LPSCC in US and French plants. Here, the values of □ (characteristic space parameter in the Weibull distribution) are in the range of 10 to 41 EFPY and the values of □ (slope or "shape factor" in the Weibull distribution) are in the range of 1.36 to 4.93 (noting that these data were analyzed with a two parameter Weibull fit). Such data suggest that the first failures occur in the range of about 0.1 of the mean. The data of Figure B.15.7, taken together and recognizing the differences in temperature, indicate that early LPSCC can occur in about a year. Details of dependencies of LPSCC are described by Staehle and Gorman.[1]

Local cold work on the secondary side, Case I--no precursor

Figure B.15.8 describes a situation in which relatively deep scratches, which were present at the start of the operation, produced local cold work that initiated extensive SCC. Staehle and Gorman[1] have summarized numerous such instances. Such SCC has penetrated the full thickness of the tubes five years after the start of operation and was found on the surfaces of the cold leg of the secondary side. Hundreds of SCC events per inch occurred on some of the scratches. The fact that such SCC initiated and propagated on the free span of the cold side attests to the severity of the initial cold work.

Figure B.15.8 shows first in (a)[12] and then (b)[12] the location of the failures. Figure B.15.8c[12] shows details of the scratch in plan view, and Figure B.15.8d[12] shows the scratch in cross section with the SCC emanating. Figures B.15.8e[13] and B.15.8f[14,15] show the accelerative effects of cold work, which supports the conclusion that local cold work started the cracks nucleating early. The scratches here seem to be deeper than most ordinary scratches from processing.

sponds to Case II of Figure B.15.1 where a relatively short (e.g. half to 20 years) precursor period precedes the evolution of the SCC itself.

## 2.1 Failures without time-dependent pre-conditions, no precursors, Case I

SCC on the primary side, LPSCC--no precursor

On the primary side of steam generator tubes there are no crevices, and the chemistry is generally constant with time. The major stressors are residual stresses and temperature; thus, any SCC that occurs does not depend on accumulation processes in a precursor period. The highest residual stresses are initially present either at small diameter U-bends or at roll transitions at the top of the tubesheet; Figure B.15.7a[10] shows data for the temperature dependence of LPSCC in the small diameter U-bends of SGs. The earliest failures at the highest temperature, about 306°C, occurred after 20-30 months. Figure B.15.7b[11] shows a cumulative distribution function (cdf) in Weibull coordinates for the LPSCC in US and French plants. Here, the values of $\theta$ (characteristic space parameter in the Weibull distribution) are in the range of 10 to 41 EFPY and the values of $\beta$ (slope or "shape factor" in the Weibull distribution) are in the range of 1.36 to 4.93 (noting that these data were analyzed with a two parameter Weibull fit). Such data suggest that the first failures occur in the range of about 0.1 of the mean. The data of Figure B.15.7, taken together and recognizing the differences in temperature, indicate that early LPSCC can occur in about a year. Details of dependencies of LPSCC are described by Staehle and Gorman.[1]

Local cold work on the secondary side, Case I--no precursor

Figure B.15.8 describes a situation in which relatively deep scratches, which were present at the start of the operation, produced local cold work that initiated extensive SCC. Staehle and Gorman[1] have summarized numerous such instances. Such SCC has penetrated the full thickness of the tubes five years after the start of operation and was found on the surfaces of the cold leg of the secondary side. Hundreds of SCC events per inch occurred on some of the scratches. The fact that such SCC initiated and propagated on the free span of the cold side attests to the severity of the initial cold work.

Figure B.15.8 shows first in (a)[12] and then (b) the location of the failures. Figure B.15.8c shows details of the scratch in plan view, and Figure B.15.8d[12] shows the scratch in cross section with the SCC emanating. Figures B.15.8e[13] and B.15.8f[14,15] show the accelerative effects of cold work, which supports the conclusion that local cold work started the cracks nucleating early. The scratches here seem to be deeper than most ordinary scratches from processing.

(a)

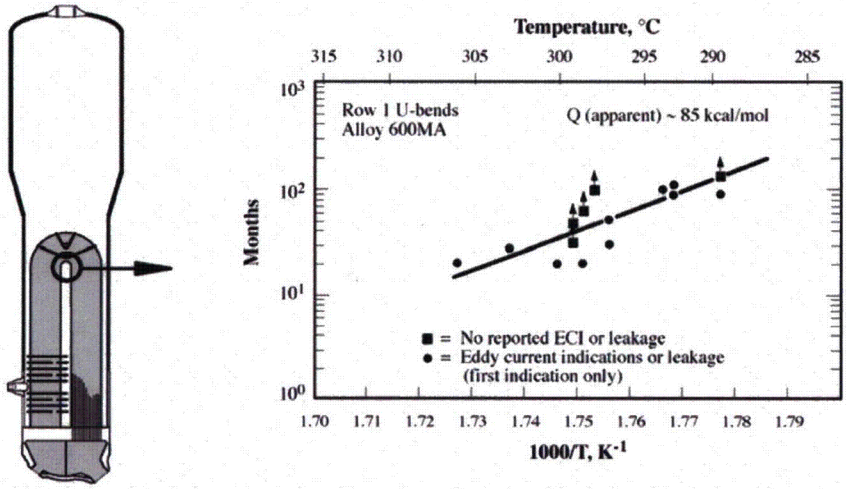


(b)

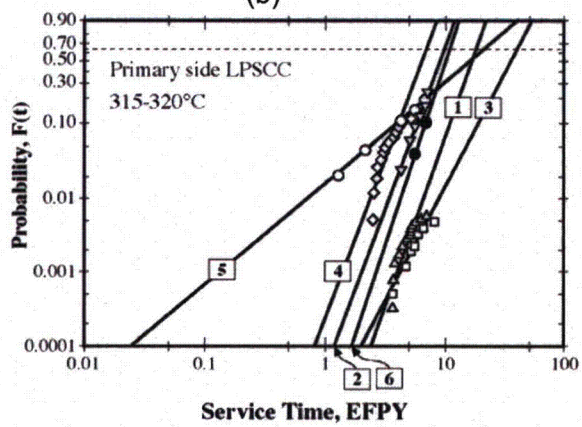


**1. French plants, LTMA tubing**
$\theta = 18.7$ EFPY
$\beta = 4.48$
$r^2 = 0.82$

**2. Part depth roll**
$\theta = 10.0$ EFPY
$\beta = 4.29$
$r^2 = 0.95$

**3. U.S.-made row 2 U-bends, French plants**
$\theta = 41.1$ EFPY
$\beta = 3.07$
$r^2 = 0.95$

**4. U.S.-made row 1 U-bends, French plants**
$\theta = 7.13$ EFPY
$\beta = 4.29$
$r^2 = 0.77$

**5. Roll transitions for kiss rolls**
$\theta = 22.23$ EFPY
$\beta = 1.36$
$r^2 = 0.98$

**6. Primary side denting**
$\theta = 10.95$ EFPY
$\beta = 4.93$
$r^2 = 1.0$

**Figure B.15.7** (a) Time-to-failure for Row 1 U-bends of PWR steam generators on the primary side. From Begley et al. Courtesy of SFEN. (b) Probability vs. service time (EFPY) for the LPSCC occurring on the primary side of tubes from operating SGs in PWRs. Temperatures in the range of 315 to 320° C. From Staehle et al.[11] © NACE International 1994.

Figure B.15.8 also shows a scenario starting with M-1 ("M" identifies a "microprocess") through M-4, i.e. from the scratch through the cold work to the SCC, as accelerated by cold work and the SCC propagating as it moves beyond the cold work. However, here, this SCC certainly began at the start of life of the plant. The scratches accelerated the initiation. The

relatively long time for perforation, compared with Figure B.15.7, results from the lower cold leg temperatures.

Flow assisted corrosion (FAC) at Mihama—no precursor

Figure B.15.9 shows a failed pipe in a section from Mihama 3 at the orifice between the #4 low pressure heater and the deaerator operating at approximately 142°C. The pipe was 560mm in diameter and the wall was 10mm thick. The flow rate of water was 22m/s at a pressure of 0.93MPa and a pH of 8.6-9.3. The failure occurred after 185,700 hours of operation. The failure resulted from flow-assisted corrosion (FAC) at a location where there had been no inspections. The resulting failure killed five people and injured four others.

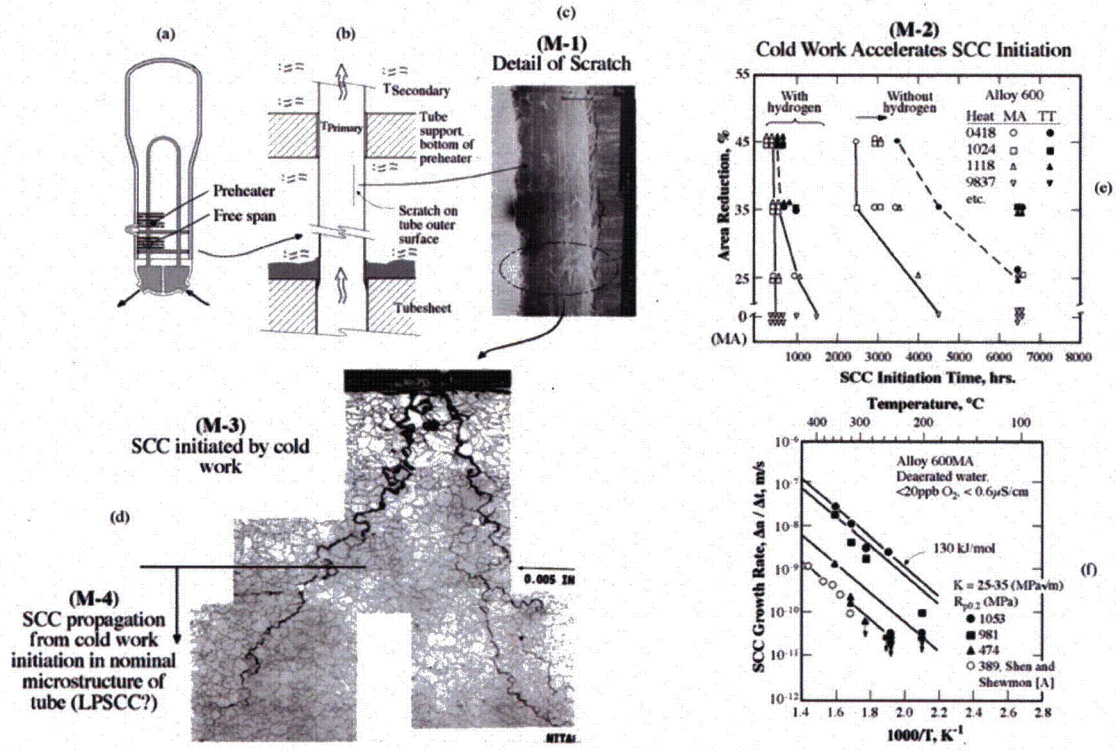


**Figure B.15.8** SCC at free-span cold leg at McGuire-2 in an Alloy 600MA tube. (a) General location of scratch and SCC. (b) Schematic view of location of SCC. (c) Detail of scratch with SEM. (d) Cross section of SCC. Courtesy of R. Eaker. (e) Area reduction vs. SCC initiation time for Alloy 600 for several heats in environments with and without hydrogen. Used by permission of EPRI. (f) SCC growth rate vs. 1000/T for Alloy 600MA with various yield strengths achieved by cold work. From Speidel and Magdowski. Courtesy of EDF. Data from [A] Shen and Shewmon.

The pipe was a thin wall large diameter pipe with high velocity water flowing at 22m/s. The FAC involved in this accident most certainly started at the initial operation and did not involve any precursor period according to Case I of Figure B.15.1. Although the FAC proceeded at a relatively slow rate, no inspections were performed up to the time of failure.

Stress corrosion cracking in sensitized and non-sensitized stainless steels in BWR applications – no precursor

Figure B.15.10 shows three examples of data for SCC in stainless steels, which are used in BWR applications. These include sensitized Type 304, non-sensitized Type 304, and stabilized Types 321 and 347. Numerous instances of SCC in non-sensitized stainless steel have occurred.[16,17,18,19] In these cases, the local environment and condition of material do not change, although low temperature sensitization could aggravate the susceptibility to SCC.

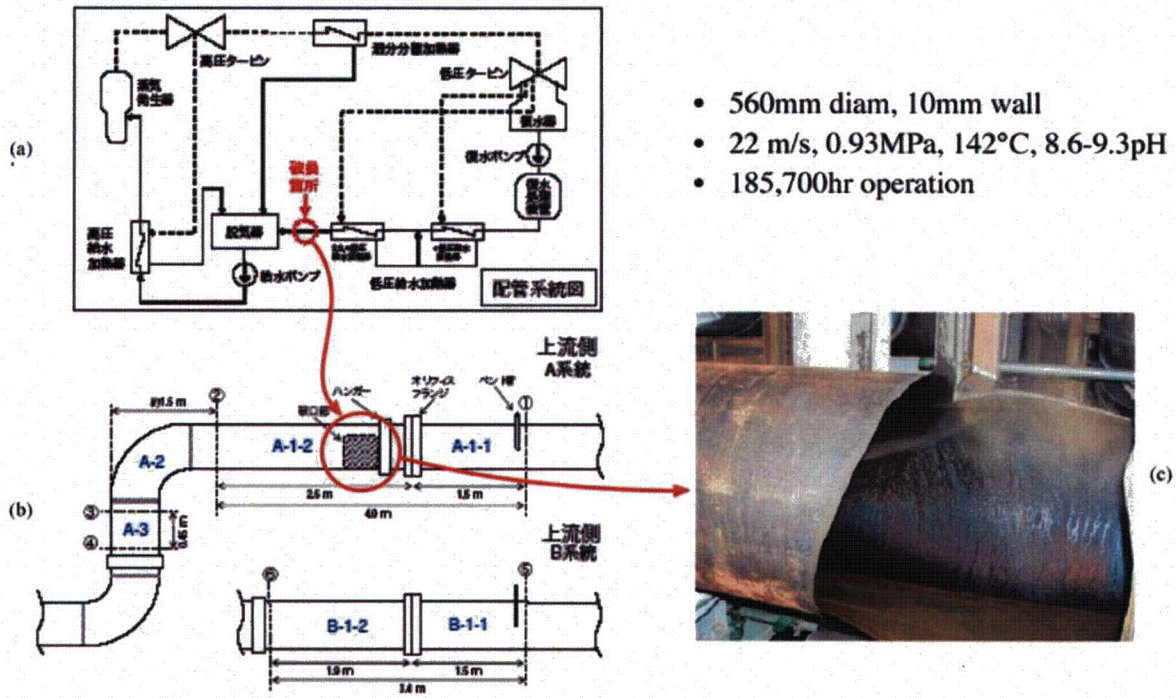


**Figure B.15.9** (a) and (b) Locations of failure. (c) Failure of pipe.

Figure B.15.10a[20] shows the probability of cracking vs. time for SCC of 2-inch and 4-inch stainless steel piping that was sensitized at welds and exposed to BWR conditions. Here, the probabilistic nature of the ultimate failures is clear, although the initiation most likely started with the beginning of operation of the plants.

Figure B.15.10b, from work by Angeliu et al.,[21] compares sensitized and non-sensitized Type 304 stainless steel in BWR environments vs. the corrosion potential and shows that the crack growth rates of the non-sensitized materials is lower than for sensitized specimens (compare the large black triangles and large black squares with the smaller data points). The circles are both for cold worked material and indicate that cold work increases the rate of non-sensitized materials significantly in the same range of potentials. The half shaded circles refer to specimens cold worked at -55°C where mainly martensite is produced; the open circles refer to specimens cold worked at +140°C where only cold worked microstructure is produced. It is clear here that cold work accelerates the SCC of non-sensitized material regardless of the

resulting microstructure. It is also clear that SCC in sensitized material proceeds more rapidly than non-sensitized material.

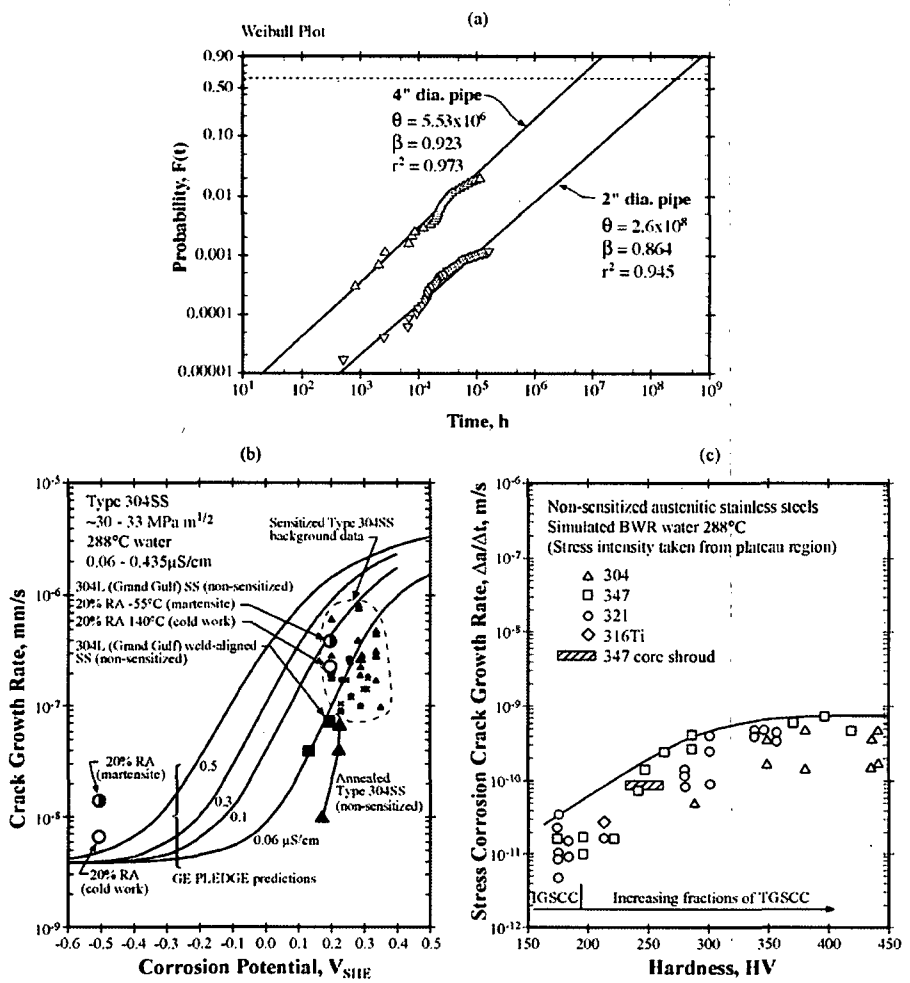


**Fig. B.15.10** SCC of stainless steels exposed to normal BWR water chemistry. (a) Probability vs. time for the failure of Type 304 stainless steels in 2- and 4-inch diameter pipes in operating plants as shown in Weibull coordinates. Failures or indications have occurred at the smooth inside surfaces associated with welds. From Eason and Shusto. *Used by permission of EPRI* (b) Crack growth rate vs. corrosion potential for stainless steels in sensitized and non-sensitized Type 304 stainless steel. Smaller symbols indicate the SCC of sensitized stainless steel from background experiments. Larger symbols indicate more recent experiments. Large triangles are for non-sensitized and annealed Type 304. Squares are for weld heat affected specimens aligned with weld; low carbon and non-sensitized. Circles are for specimens with 20% reduction in area. The half shaded specimen was deformed at -55°C to produce mainly martensite. The open large circle is for cold work at 140°C to achieve only cold work. From Angeliu et al. (c) Crack growth rate vs. hardness for non-sensitized stainless steels. From Speidel and Magdowski.[22] *Reprinted with permission from TMS*

Figure B.15.10c, from work by Speidel and Magdowski,[22] compares Type 304 with stabilized stainless steels and with a core shroud as a function of hardness. Here, the trend in Figure B.15.10b is corroborated and extended.

## 2.2 Failures with significant but relatively short precursor times, Case II.

In this section, examples of failures are described where the SCC is preceded by a precursor step, as shown in Case II of Figure B.15.1. These examples suggest how such precursors might arise and proceed.

ODSCC at tubesheets and tube supports--precursor

Figure B.15.11 shows successive steps (M-X) leading to SCC on the outside diameter of SG tubes in heated crevices. The precursor steps involve at least the following:

a. Build-up of deposits in crevice (M-1).

b. Concentration of chemicals in heat transfer crevices (M-2).

c. Further concentration and chemical reactions inside the crevices (M-3).

Then, the resulting SCC, as shown at (M-4), can initiate. This precursor process is not lengthy, but the overall process is nonetheless a Case II process with a precursor preceding the initiation of SCC.

Denting associated with tubesheets and tube supports--precursor

Figure B.15.12 shows an integrated view of the denting processes as they may occur at tube supports or at the top of the tubesheet and as related to previous experimental work of Pickering et al.[23] and Pilling and Bedworth.[24] The precursor steps for denting are much like the ODSCC in Section 2.2-1. The precursor steps involve at least the following:

a. Build-up of deposit in crevice (M-1).

b. Concentration of chemicals in the heat transfer crevices (M-2).

c. Corrosion products expand, according to the predictions of Pilling and Bedworth, as the carbon steel of the tube supports corrodes. These corrosion products produce stresses (M-3), as measured by Pickering et al., in the tube wall and cause it to deform (M-4).

The straining of the tube, after the corrosion products expand, produces SCC from both inside and outside of the tubes (M-5). Such SCC has not been observed associated with denting at the top of the tubesheet, but such a result is possible. From the analysis of Staehle and Gorman, based on extensive work described in the literature, it appears that the growth of the oxide was particularly influenced by the presence of chloride and copper in the secondary environment. Thus, improving the integrity of the condensers and changing the condenser materials from copper-base alloys to titanium were the main avenues for mitigation.

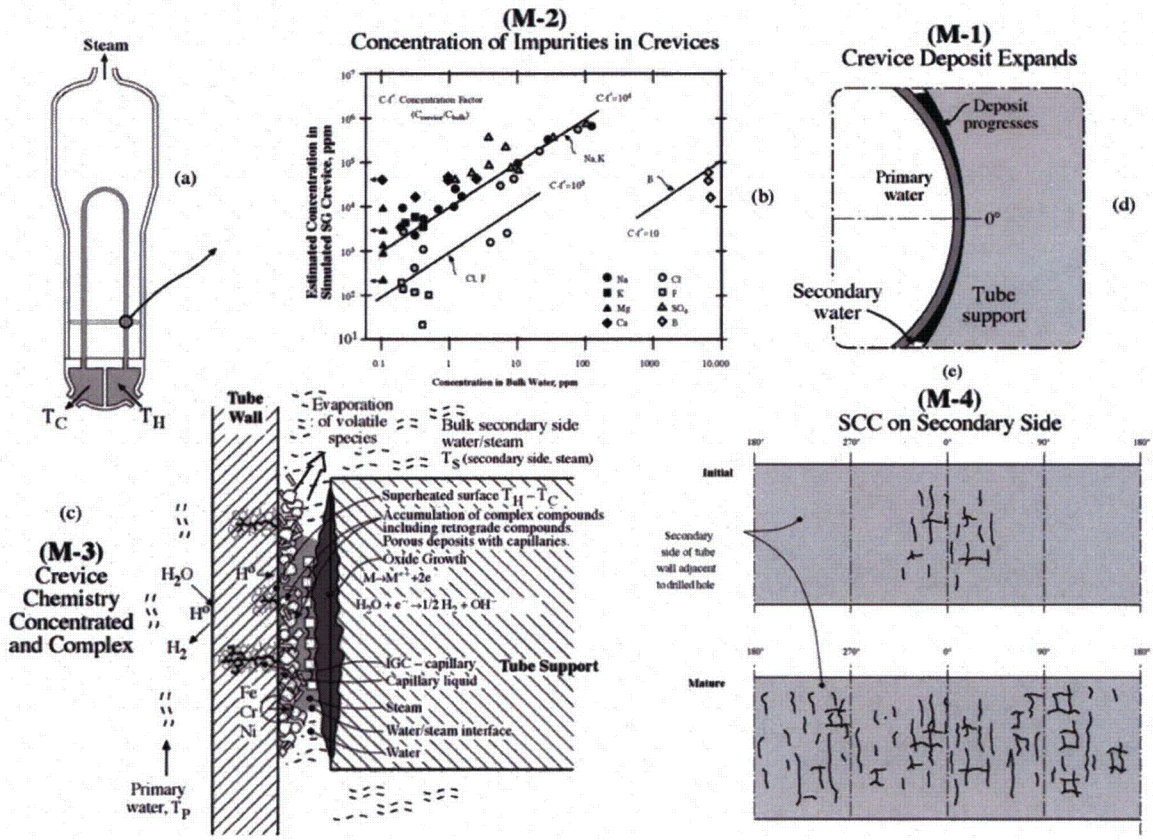


**Figure B.15.11** Steps involved in the SCC on the OD of a tube associated with a drilled hole geometry of an Alloy 600-tubed steam generator.

<u>SCC in OTSG upper bundle--precursor</u>

SCC has occurred in the upper bundles of SGs where the steam is progressively superheated. While this SCC appears to be mostly focused at scratches, SCC and IGC occur outside these scratches to a lesser extent. The tube material is Alloy 600SR (stress relieved). Figure B.15.13a[25] shows the composition of various parts of the surface and SCC. It appears that the design of these OTSG units assumed that the water would be so pure that such accumulations of chemicals would not occur and would certainly not damage the tubes. The SCC was quite extensive in the superheated region. Figure B.15.13b[26] shows the tubes plugged vs. time. Significant tube plugging started after 12 years in 1986. The precursor step is comprised mainly of the accumulation of chemicals on the surfaces until a sufficient amount of chemicals is present. The precursor period appears to have been about 10-12 years.

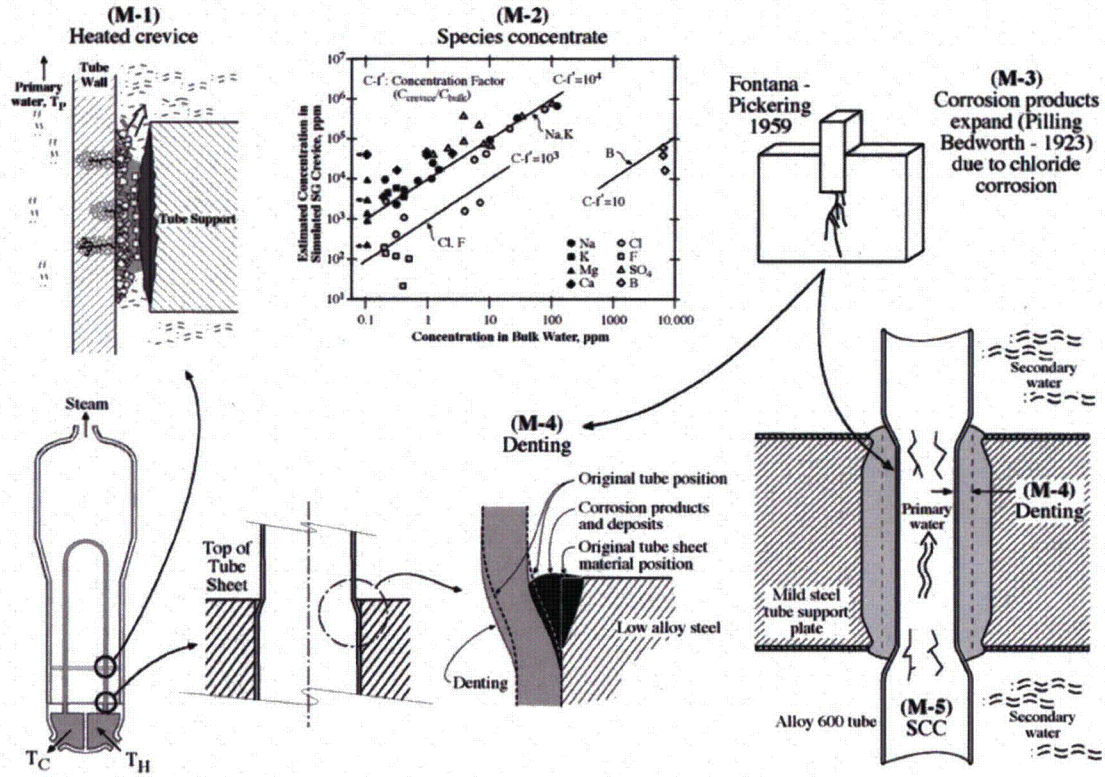


**Figure B.15.12** Steps in the development of denting at both tube supports and at the top of the tubesheet. The straining is shown at the tube supports to have produced SCC starting from both inside and outside surfaces.[23,24]

<u>Fuel failures in BWR plants--precursor</u>

Fuel failures in BWR plants seem to be occurring as the heat flux increases with increasing demands for high outputs. The failure is not SCC, but rather a corrosion perforation. However, the precursor process is useful to analyze here. The precursor steps, as summarized in Figure B.15.14, are mainly:

a. High, and increasing, heat flux (M-1).

b. Impurities that participate in forming deposits with higher heat transfer resistance (M-1).

c. Increase in corrosion rate and formation of thicker oxide with higher heat transfer resistance (M-2).

d. Deposition of impurities and growth of oxide produces higher surface temperatures that accelerate perforation of cladding (M-3).

e. The cladding then perforates (M-4) as illustrated in Figure B.15.14d. This process occurs within a fuel cycle and is therefore a several year process.

Davis Besse--precursor

In the case of the Davis Besse failure, as shown in Figure B.15.15, LPSCC was part of the precursor, rather than the terminal part, and an extensive volume of corrosion ensued after an SCC-incited leak occurred in a control rod drive nozzle. The precursor elements were:

a. High residual stresses due to welding (M-1).

b. LPSCC in the Alloy 600MA nozzle (M-2).

c. Perforation of the Alloy 600MA permits borated water to exit and produce both a high velocity and corrosive solution (M-3).

The corrosion rate of the steel is about 2" per year and consumes a volume of steel that is the thickness of the head and about 6" in diameter. The precursor time, i.e. the time for the LPSCC to perforate the wall of the nozzle, was about 18 years, which is comparative to the rate for SG tubes when the differences in thicknesses are accounted for.

## 3. Structure of Domains and Microprocesses – Approach to Quantifying Precursors of Case III

### 3.1 Introduction

The purpose of this section is to describe the structure and application of "domains" and "microprocesses," as used in developing scenarios that are part of the precursor events that precede initiating SCC as shown in Figures B.15.1, B.15.5 and B.15.6. This discussion is the essence of the approach to quantifying precursors for Case III. Figures B.15.16 through B.15.21 describe each of the domains, which are identified in Figures B.15.5 and B.15.6, together with examples of relevant microprocesses.

Again, the purpose of this report is to propose an approach to predicting failure processes, mostly SCC, that have not yet been observed. In order to develop such a prediction, a rational intellectual structure and some assumptions are necessary. The intellectual structure is discussed in this section in terms of the domains and microprocesses. The principal assumptions and features of this intellectual structure are:

- Predicting failures, which have not yet occurred, is mostly related to long term changes in the domains and microprocesses, which are precursors, as described in Figure B.15.1 and Figure B.15.6, and which enable SCC to initiate and propagate at later times.

- Some new mode of SCC is not reasonably expected. It is more likely that the development of the precursors will permit some existing failure process to occur rather than some totally new one.

- The development of precursor conditions depends on the progression of microprocesses in various domains, as shown in Figure B.15.5, which may act conjointly or individually.

- The choices of specific domains and microprocesses must be based upon experience, and an awareness of the wide varieties of microprocesses that can be important.

- The idea of microprocesses focuses on specific processes that occur within the domains and have been shown to be critical processes in the nucleation, initiation, and growth of SCC. Further, these microprocesses are often capable of being quantified by known procedures of analysis.

- Finally, the domains and microprocesses can be linked to a scenario for the development of critical conditions for the initiation and propagation of SCC or a similarly aggressive process. Several scenarios could be envisioned as options for precursors. Section 7.0 provides suggestions for failure processes that might be predicted with the MPSA approach.

### 3.2 The "domains"

The "domains" in this discussion are shown in Figure B.15.5. These domains provide an intellectual framework for identifying explicitly the sequence of events and for organizing the microprocesses.

A sample scenario that might constitute a precursor to SCC could be the following:

a. Microprocess #1 (M-1): A line-contact crevice slowly accumulates deposit.

b. Microprocess #2 (M-2): The deposit gradually hardens.

c. Microprocess #3 (M-3): Even dilute species in the bulk water concentrate in the crevices.

d. Microprocess #4 (M-4): Metallurgical ripening over time increases slip coplanarity leading to sharper slip steps and greater local forces at internal barriers.

   These first four steps constitute a precursor as shown in Figure B.15.1, and may require many years.

e. SCC initiates when the environment in the crevice interacts with a metallurgical slip of greater coplanarity in the metal substrate.

Starting from the overall schematic view in Figure B.15.5, where the adjacent domains are identified and shown adjacent to a schematic cross-section of a metal in an aqueous solution, the respective domains are described in Figures B.15.16- B.15.21. These domains, as identified in the Figures, start from the global domain to the bulk metal according to the order in Figure B.15

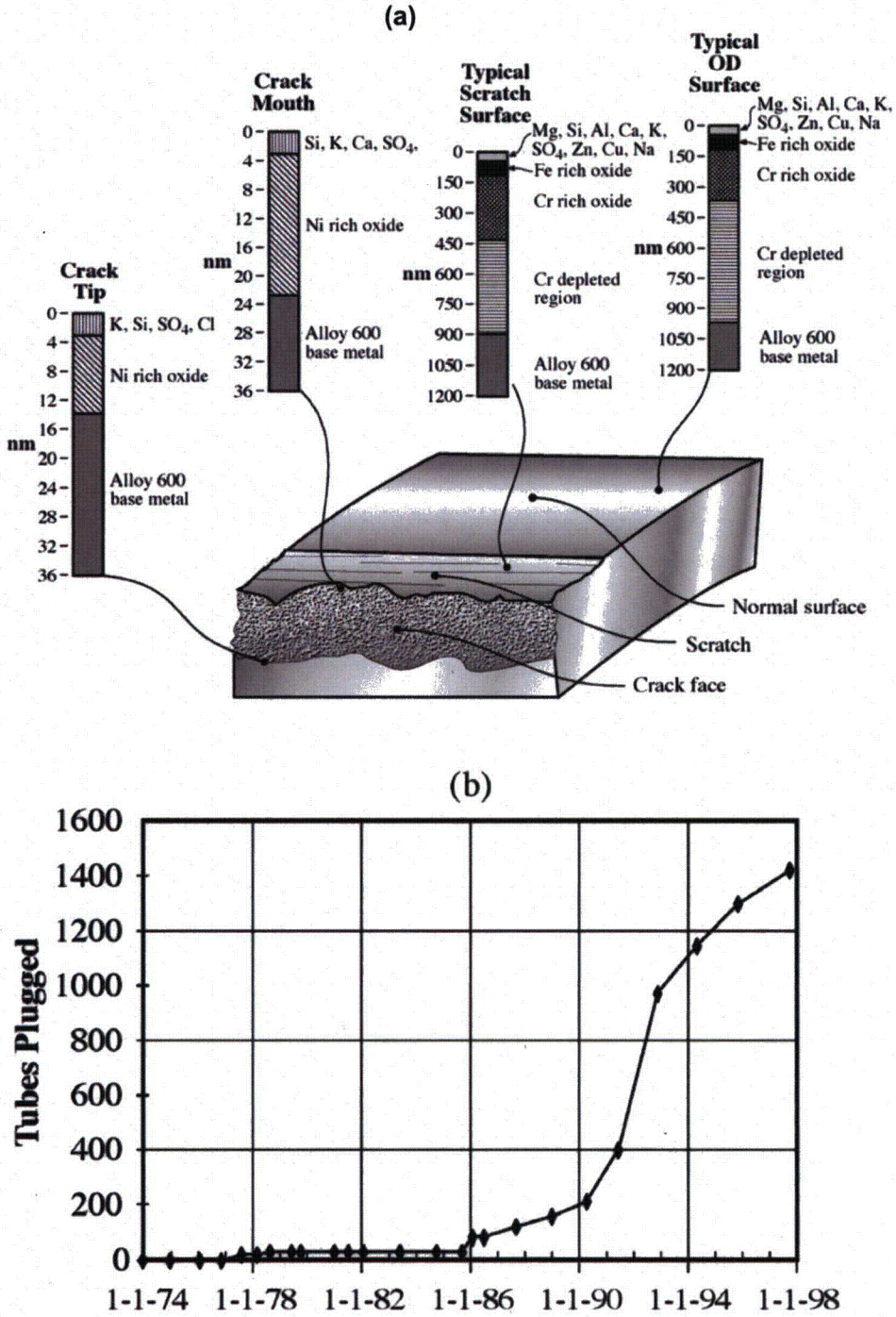


**Figure B.15.13** (a) Compositions of surfaces of tubes at four locations in the upper bundle of Oconee Nuclear Station. Outside surfaces and inside SCC and IGC as determined by Auger spectroscopy. From Rochester.[25] Reprinted with permission from BNES. (b) Tubes plugged vs. time for Oconee-1B. From Rochester and Eaker.[26] Reprinted with permission from TMS.

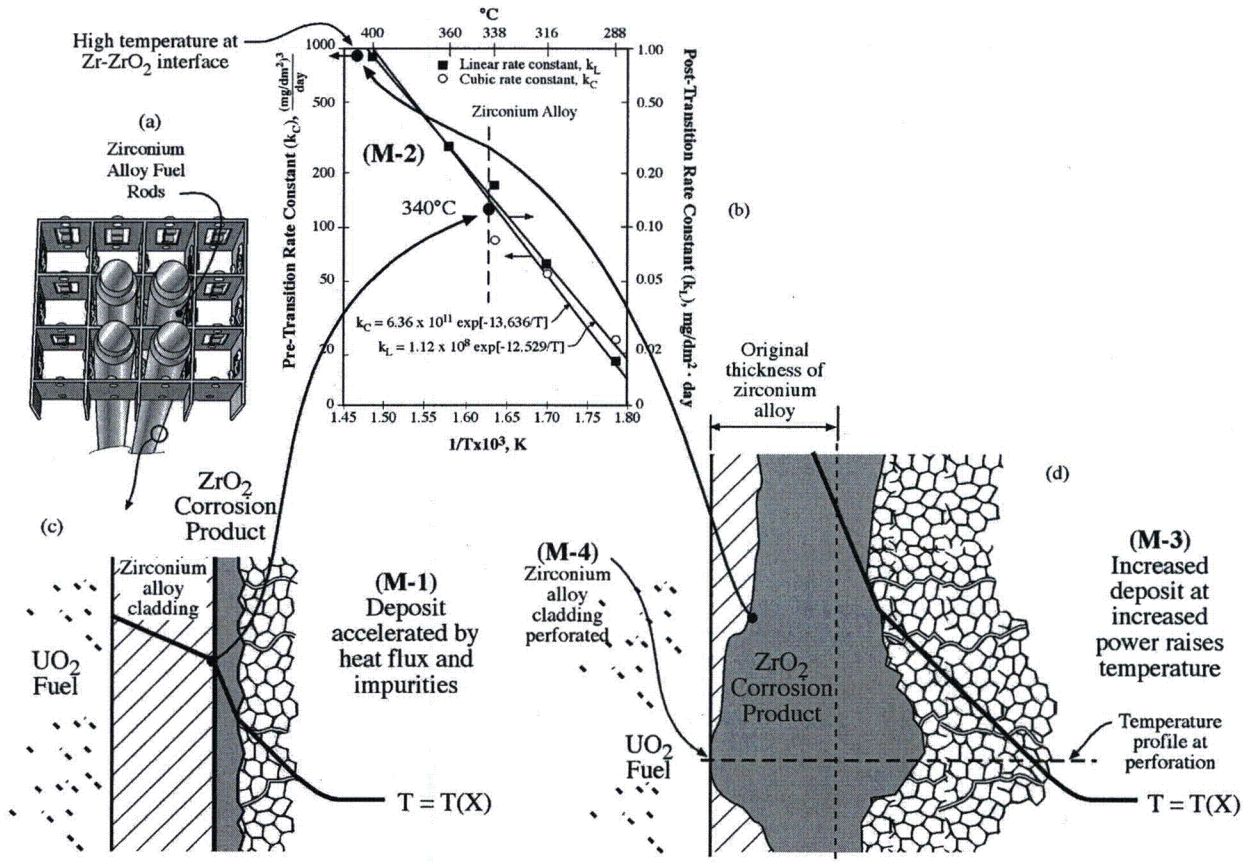


**Figure B.15.14** Stepwise process for the perforation of fuel that results first from deposits, the formation of which is accelerated by high heat flux (M-1), then by accelerated corrosion (M-2), then by progressively higher surface temperatures (M-3), thereby increasing the corrosion rate, and ultimately failure (M-4).

Each of the domains consist of the "microprocesses" that are shown at the left, and some examples of nominal effects are identified at the right. These microprocesses are the elements, which contribute to the precursor, that would be quantified.

The "Global Domain" is shown in Figure B.15.16. The Global Domain is intended to include microprocesses that apply to all the domains, (e.g. temperature, neutron flux). The Global Domain also includes the free energy change, ΔG, as the environment reacts with the metal to produce reaction products.

The "Bulk Environment Domain" is shown in Figure B.15.17. The Bulk Environment Domain refers to the primary water, the secondary water, steam, tertiary water, ambient inside the containment or outside, and similar fluids to which components and materials are exposed.

The "Near-Surface Environment Domain" is shown in Figure B.15.18. The Near-Surface Environment Domain consists mainly of deposits, flow gradients, MIC pustules, and electrochemical cells. Such a domain has been a main part of the crevice deposits on the secondary side in heat transfer crevices or the accumulation of sludge at the top of the tubesheet in SGs.

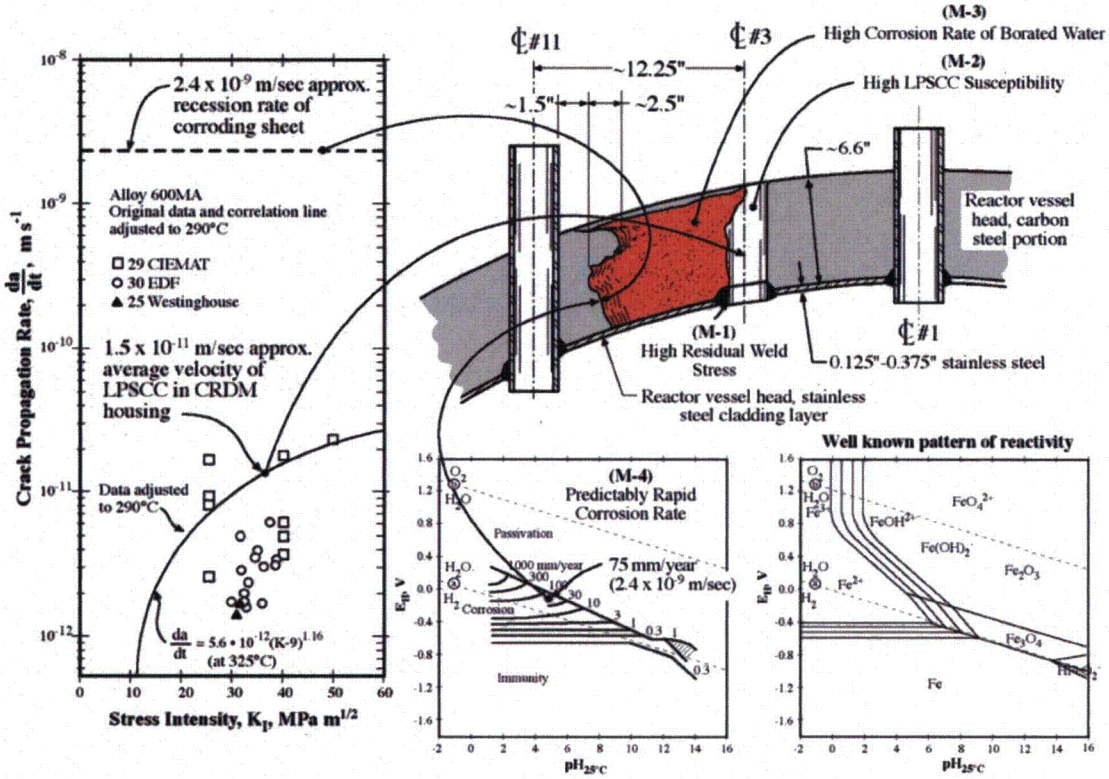


**Figure B.15.15** Stepwise process leading to the failure at Davis-Besse. Here, LPSCC was part of the precursor, and rapid general corrosion was the propagation process. The LPSCC started with the high residual stresses from welding and the already well-known susceptibility of the Alloy 600MA.

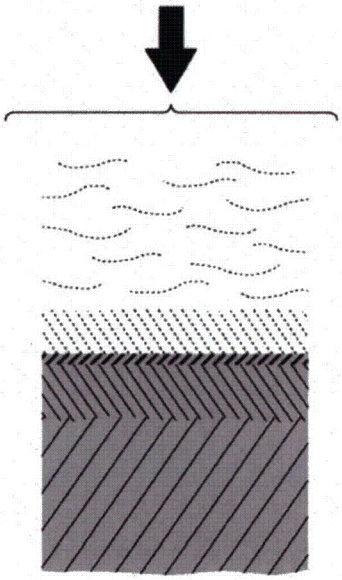

## Global Domain

| Microprocesses (Time Related) | Effects |
|---|---|
| 1. Component in system | • Produce products that damage other components<br>• Products from other components damage subject components |
| 2. ΔG - Overall free energy change: environmental chemistry (pH, $H_2O$, $O_2$, $H_2$, $N_2H_4$) to material (Fe, Ni, Cr, Cu, Ti, . . .) | • Driving force for chemical reactions<br>• Boundaries for SCC modes |
| 3. Ambient temperature | • Reaction rates<br>• Thermal stresses |
| 4. Heat Flux | • Surface deposits<br>• Surface temperatures |
| 5. Cyclic stresses (Cyclic Frequency) | • Fatigue, corrosion fatigue |
| 6. Crevices | • Accumulation of chemicals<br>• Stress intensity |
| 7. Irradiation | • Local differences<br>• Voids<br>• Radiolysis |

**Figure B.15.16** Microprocesses and their effects in the Global Domain.

The "Protective Film Domain," which is shown in Figure B.15.19, includes what is sometimes called the "passive film." However, there are other deposits that form as part of the protection, (e.g. carbonates), and are not part of the chemistry of the metal substrate. In the protective film, the electrochemical catalytic processes are affected as the defect structure of the protective film changes – such defect structures are changed by Pb, $Cl^-$, $S^{2-}$ and others. Because this film is usually epitaxially attached to the surface, the protective film also affects both stresses in the substrate and the nucleation of dislocations at the surface. This film changes with time in its geometry and chemistry.

## Bulk Environment Domain

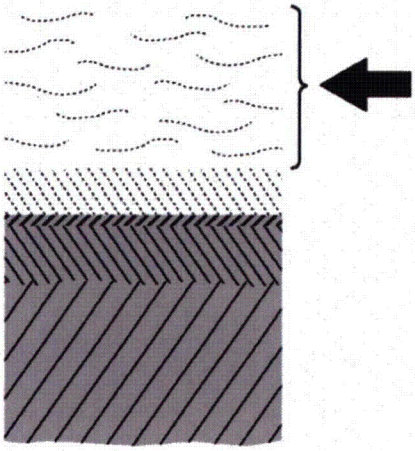

| Microprocesses (Time Related) | Effects |
|---|---|
| 1. Flow | • Transports chemical and suspended solids<br>• Influence rates of surface reactions<br>• Low flow / high flow deposits solids<br>• FAC |
| 2. Boiling | • Deposit solids |
| 3. Transport to or from other components | • $Cu^{2+}$, $HS^-$ |
| 4. Chemical composition<br>• $O_2$, $H_2$, $N_2H_4$ impurities (Pb, $Cl^-$, $SO_4$), pH inhibitors, suspended solids | • Electrochemical state<br>• Corrosion reactions<br>• Raise E with low $H_2$ |
| 5. Homogenous chemical reactions | • Reduce $SO_4^= \rightarrow HS^-$ with $N_2H_4$ |
| 6. Radiolysis and radiolytic synthesis | • $H_2O \rightarrow O_2 + H_2$<br>• $N_2 + H_2O \rightarrow HNO_3$<br>• $O_2 + N_2H_4 \rightarrow H_2O$ |
| 7. Multiple oxygen incidents | • Corrosion<br>• SCC |

**Figure B.15.17** Microprocesses and their effects in the Bulk Environment Domain

The "Near-Surface Domain on the Metal Side," which is shown in Figure B.15.20, is the region in which near-surface processes occur such as slip dissolution, tunnel penetration, enrichment/depletion of species, solubilization of species that enter grain boundaries, and precipitation of vacancies.

## Near-Surface Domain (Environment Side)

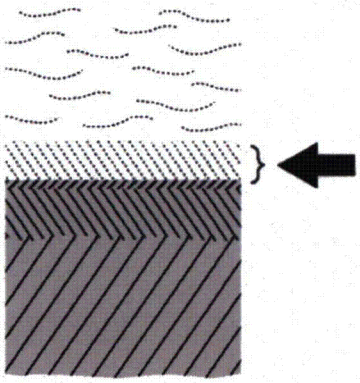

| Microprocesses (Time Related) | Effects |
|---|---|
| 1. Deposits | • Corrosion cells<br>• Heat transfer resistance<br>• Galvanic processes |
| 2. Heat flux | • Concentrate chemicals<br>• Raise surface temperatures |
| 3. Sequestering, crevices | • Concentrate chemicals |
| 4. FAC | • Remove material<br>• Produce hydrogen<br>• Inhibit initiation of SCC |
| 5. MIC | • Act at temperatures below 100°C<br>• Acidic and other corrosive environments |

**Figure B.15.18** Microprocesses and their effects in the Near-Surface Environment Domain

## Protective Film Domain

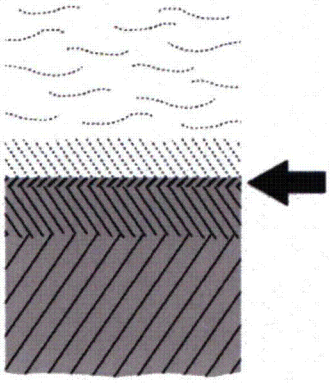

| Microprocesses (Time Related) | Effects |
|---|---|
| 1. Thickness | • Surface stress<br>• Heat transfer |
| 2. Composition (environment contribution, alloy contribution, defect structure, xtal/amorphous) | • Conductivity<br>• Pit nucleation<br>• SCC initiation |
| 3.Stresses (average, metal interface) | • Film degradation |
| 4. Kinetics (repassivation, dissolution, growth) | • Local penetration<br>• Slip dissolution |
| 5. Slip interactions | • Slip height<br>• Step distribution<br>• Dislocation nucleation |

**Figure B.15.19** Microprocesses and their effects in the Protective Film Domain

## Near Surface Domain (Metal Side)

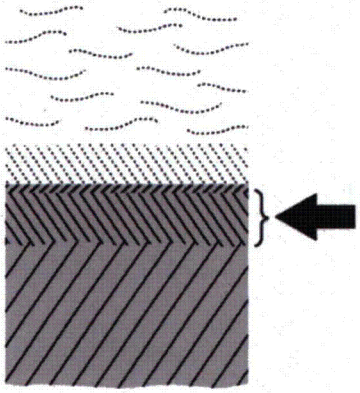

| Microprocesses (Time Related) | Effects |
|---|---|
| 1. Enrichment/depletion | • Brittle layer<br>• Catalysis<br>• Change chemistry into SCC mode<br>• Galvanic<br>• Voids |
| 2. Hydrogen entry | • SCC |
| 3. Surface slip | • SCC initiation |
| 4. Grain boundary (composition, diffusion) | • IGC<br>• G.B. diffusion |
| 5. Irradiation-induced voids | • Stresses, distortion |
| 6. Slip dissolution | • SCC initiation |
| 7. Tunnels | • SCC initiation |
| 8. General dissolution | • Surface recession |
| 9. Pits, IG corrosion, electrochemical cells | • Penetration<br>• CF initiation |
| 10. SCC initiation | • Accelerate |
| 11. FAC | • Recession<br>• Remove SCC initiation<br>• Hydrogen production |
| 12. Abuse (dings, dents, machining, grinding) | • SCC initiation |

**Figure B.15.20** Microprocesses and their effects in the Near-Surface Metal Domain

The "Bulk Metal Domain," which is shown in Figure B.15.21, is, in a sense, the "semi-infinite region" of the metal, which, on a gross scale, is homogeneous but on a microscopic—and microprocess scale—is quite heterogeneous. These local heterogeneities provide paths or influences that affect the development and propagation of corrosion damage.

The six domains of Figures B.15.16 through B.15.21, as summarized in Figure B.15.5, are shown with associated small boxes in Figure B.15.6, each of which represents a microprocess. When a "scenario" is constructed as in Figure B.15.6, these boxes are connected, as they would be naturally. Such a scenario constitutes a precursor as shown in Figures B.15.1 and B.15.6 that identifies the relevant microprocesses, which need to be quantified and validated in order to

reach the conditions necessary for SCC to initiate. In this quantification, some kind of time dependence needs to be developed in order to predict when the resulting precursor can lead to the start of SCC.

**Bulk Metal Domain**

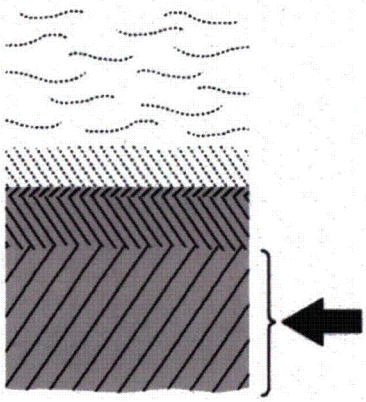

| Microprocesses (Time Related) | Effects |
|---|---|
| 1. G.B. composition, ppt | • Grain rotation<br>• Grain shedding |
| 2. G.B. composition, adsorb/desorb | • Preferential dissolution, diffusion |
| 3. G.B. diffusion ($O_2$, $N_2$, C, ...) | • Embrittlement |
| 4. G.B. movement, slip, rotation | • Break protective films |
| 5. G.B. pile-up site for dislocation-induced stresses | • Promotes IGSCC, SCC |
| 6. G.B. bubble formation ($CH_4$, $NH_3$) | • Promotes SCC |
| 7. G. matrix - early precipitation | • Promotes slip coplanarity |
| 8. G. matrix - transformation | • Promotes slip coplanarity |
| 9. G. matrix - slip coplanarity | • Pile up stress |
| 10. G. matrix - voids nucleation | • Stress |

**Figure B.15.21** Microprocesses and their effects in the Bulk Metal Domain

## 4. Examples and properties of microprocesses

The purpose of this section is to describe examples of microprocesses, which are part of the six domains. This description is not comprehensive but illustrative; there are probably 50-100 really significant microprocesses that might be identified.

As shown in Figures B.15.11- B.15.16, each domain contains a particular array of microprocesses, which are significant to the occurrence of corrosion damage. Many of these microprocesses are already known to participate in corrosion processes under various conditions of temperature, stress, environmental chemistry, and material chemistry.

The emphasis here is upon microprocesses that require some time to develop their roles in accelerating or intensifying future and aggressive corrosion; and during these early processes of development there is no support for SCC or other accelerated processes until certain necessary conditions conglomerate. Once some critical array of microprocesses develops, SCC can then initiate and propagate.

The "microprocesses" are the elements that are identified, quantified, and connected in scenarios to develop the characteristics of the precursor regimes as follows:

Identification

Identifying the microprocess in a domain, as in Figure B.15.6, is largely a matter of expert experience. Some of these microprocesses are well known and some maybe not. To identify further clues to microprocesses that are not obvious, it may be necessary to look into the physical and organic chemistry of homogenous materials and the surface chemistry of their interfaces in aqueous solutions. Other microprocesses might be identified from metal physics. "Identification" is a matter of making microprocesses explicit.

Quantification

Quantification of microprocesses provides bases for the dependencies that determine the duration of the precursor period. Such dependencies include considerations of growth rates, diffusion, rates of transformation, rates of accumulation, and rates of production. These can usually be approached with conventional knowledge of such processes as they respond to the temperatures and chemistries of LWRs. Developing the rates of microprocesses contributes to an overall model of a time-dependent precursor. From this model, the duration of the precursor can be calculated.

Connection into scenarios

Constructing a scenario, as in Figure B.15.6, involves essentially developing the features of the precursor. There may be several equally attractive scenarios. A scenario is shown schematically in Figure B.15.6, including selected microprocesses. Figure B.15.6 suggests that there may be several important microprocesses in some domains. A fully identified and connected scenario, as in Figure B.15.6, then, is a precursor to the occurrence of starting SCC or some similarly rapid process of penetration.

Note that FAC is probably not compatible with the development of these microprocesses since it starts from the beginning of operation, unless there is a change in velocity, pH, potential, inhibitors, or alloys that would activate the flow acceleration at some later time. However, FAC generally proceeds at a rate that is similar to the low end of SCC; and FAC might be initiated at a later time as a result of changes in chemistry (changes in oxygen or pH), temperature, and flow. This sequence is not so much a precursor as a later and influential change in operation.

## 4.1 Global Domain

A schematic view of the Global Domain is shown in Figure B.15.16. In Section 4.1 three examples of microprocesses are discussed, and a more extensive set is suggested in Figure B.15.16. Each of these examples is typical of important effects that could change the conditions for onset of SCC. Further, they are associated with the kinds of times that are involved with precursors that could lead to SCC at long times.

Mode diagrams, ΔG

One example of a microprocess here is the free energy difference between the environment and the material. This is usually identified by a diagram of potential vs. pH as shown in Figure B.15.22, and much of the necessary data are available in handbooks containing thermodynamic data. Here, the Ni-$H_2O$ diagram is shown with some of the Fe equilibria. Superimposed on this diagram are the locations of the major submodes of SCC. This diagram represents the global domain where the lines in the diagram indicate equilibria for the metal and environment that react to produce chemical products. The application of this diagram and the incorporation of submodes of SCC have been described by Staehle and Gorman.[1] Such a global microprocess as the difference in free energy of metal and water, is important to virtually all of the scenarios.

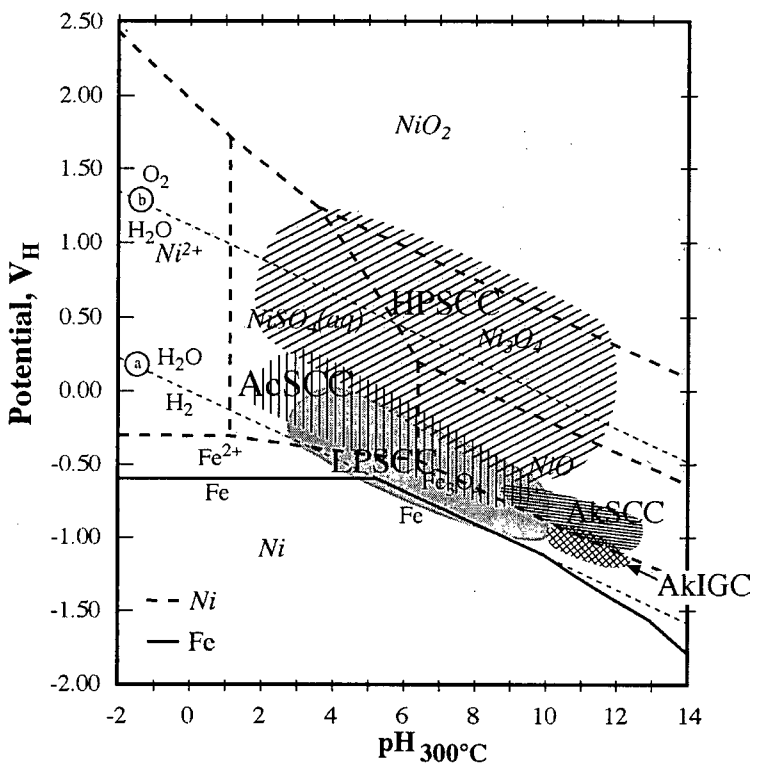


**Figure B.15.22** Electrochemical potential vs. pH at 300°C for Ni in $H_2O$ with important equilibria shown. Locations for AkSCC, LPSCC, AcSCC, and HPSCC of Alloy 600MA shown. From Staehle and Gorman.[1] © NACE International 2003/2004.

Neutron flux, void formation

Neutrons, as they react with Ni isotopes, produce helium atoms. These helium atoms coalesce to produce voids. Such voids are shown in Figure B.15.23[27] in baffle bolts. These voids, as they coalesce, lead to strains that cause stresses and distortions.

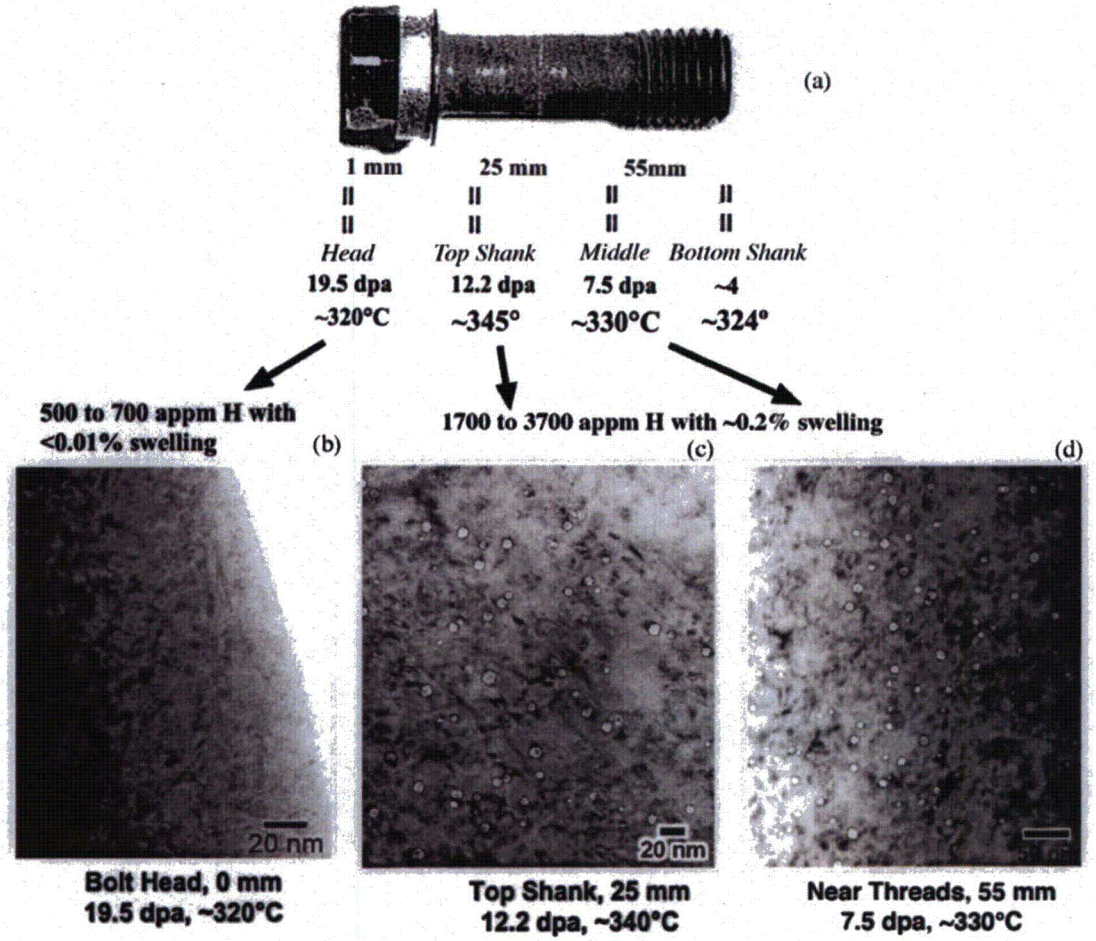


**Figure B.15.23** Bolt connecting former and baffle from Tihange-1 PWR shown in terms of neutron dose giving concentration of He and swelling at locations along a bolt. From Garner et al.[27] Reprinted with permission from TMS.

Neutron flux, change composition of grain boundaries

A third example of a microprocess in the global domain is neutron flux, as it leads to changes of chemistry at grain boundaries. Figure B.15.24[28], from the work of Bruemmer, shows such a change of Cr in stainless steel after up to 13.3 dose per atom. These alterations affect the reactivity of the grain boundaries as well as changing the mechanical properties and diffusivity of environmental species such as oxygen.

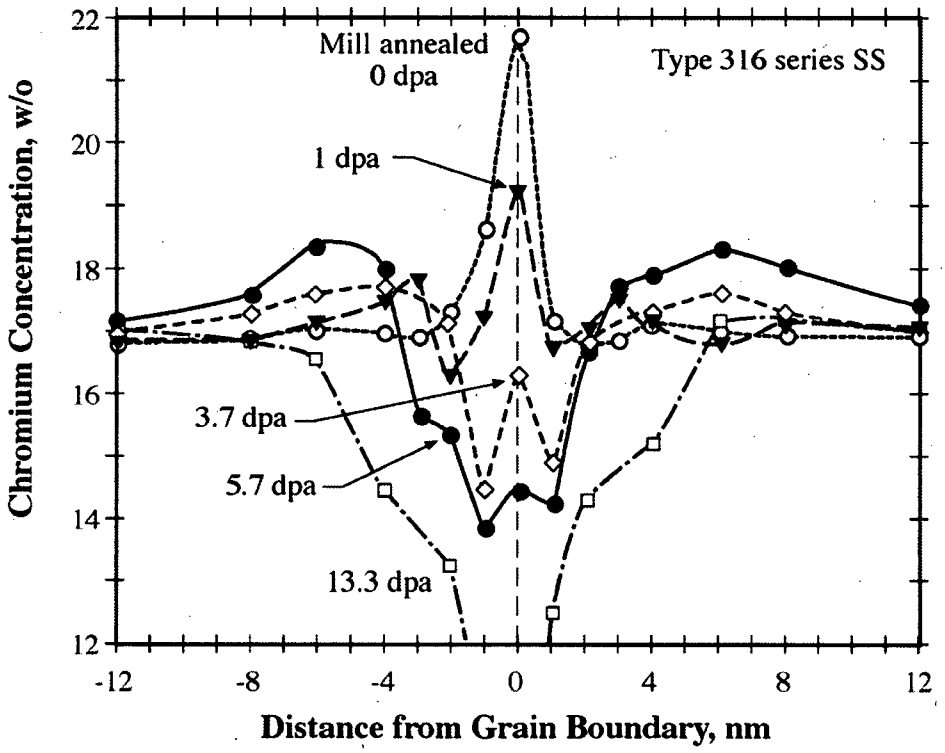


**Figure B.15.24** Concentration of Cr across a grain boundary of mill-annealed Type 316 stainless steel as a function of dose up to 13.3 dpa. From Bruemmer.[28] © NACE International 2002.

### 4.2 Bulk Environment Domain

A schematic view of the Bulk Environment Domain is shown in Figure B.15.17, where several microprocesses are identified. This section gives two examples of such microprocesses.

Hydrazine ($N_2H_4$) reduces sulfate to sulfide

Hydrazine ($N_2H_4$) is added to the secondary side of SGs in order to reduce the concentration of oxygen that is assumed to promote SCC in crevices. As an aside, it is not clear that such an effect is important; and second, the very low hydrogen on the secondary side raises the potential, regardless. Whether hydrazine significantly counters this effect of low hydrogen is not clear.

Work by Daret, et al.[29] shows that the occurrence of sulfide produces SCC in Alloy 600MA, as shown in Figure B.15.25; further, this work is linked to the reduction of sulfate in secondary systems by hydrazine as shown in the reactions of Figure B.15.25. Work by Sakai et al.,[30] Sala et al.,[31] Allmon et al.,[32] and de Bouvier et al.[33] have shown clearly that $N_2H_4$ reduces $SO_4^{2-}$ to $S^{2-}$.

Chloride inhibits dissolution

The rate of dissolution of high nickel alloys is very much affected by the anion as shown from work of Cullen in Figure B.15.26a[34]. Here, the dissolution of these alloys over a pH range from 1-6 is shown for several ratios of chloride and sulfate including the 100% compositions of each. These data show that the 100% chloride solution corrodes Alloy 600 about two orders of magnitude less than the 100% sulfate. In support of this trend, Figure B.15.26b[35] from Choi and Was, shows that the aspect ratio of pitting follows the same pattern. As the chloride-to-sulfate ratio increases, the pits become sharper, which is expected in view of the inhibitive effect of $Cl^-$ as suggested in Figure B.15.26c from Staehle.[36]

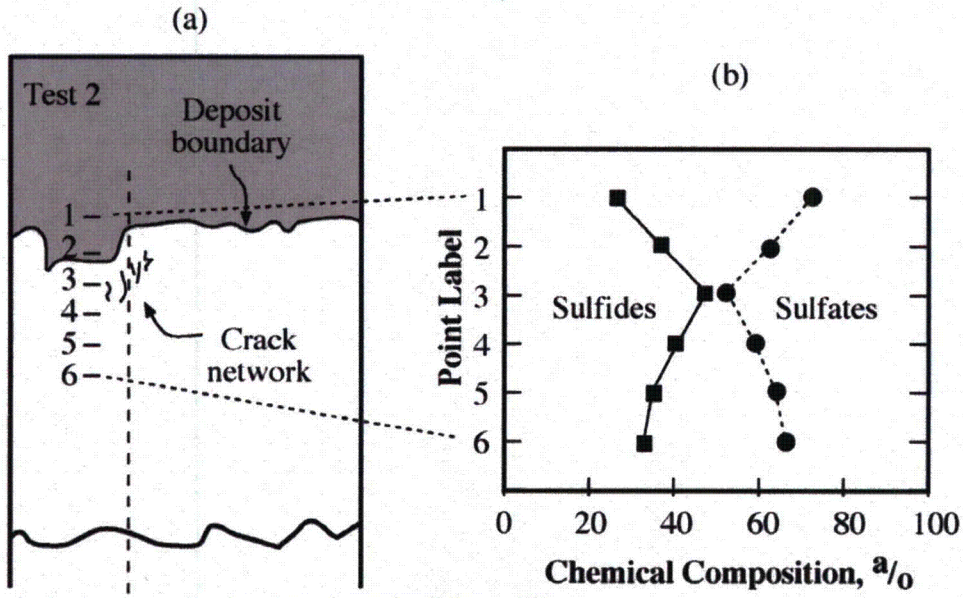


Sulfate is reduced to $S^{2-}$ by hydrazine

$$2(SO_4)^{2-} + 18H^+ + 12e^- \rightarrow 2(HS^-) + 8H_2O$$

Hydrazine is oxidized

$$3(N_2H_4) + 12OH^- \rightarrow 3N_2 + 12H_2O + 12e^-$$

**Figure B.15.25** Results from model boiler experiments with primary temperature in range of 330 to 350°C and secondary side temperatures in the range of 290 to 295°C with AVT chemistry. Sodium sulfate was added at 0.5 mg/kg in makeup water, and hydrazine was in the range of 10-50 µg/kg. Dissolved oxygen less than 1 µg/kg. (a) Location of SCC, boundary of deposit, and locations of analysis for sulfates and sulfides (1-6) for Alloy 600MA. (b) Atomic percent of sulfates and sulfides vs. distance from the boundary of the deposit into the metal and through the SCC zone. From Daret et al.[29] Reprinted with permission from TMS.

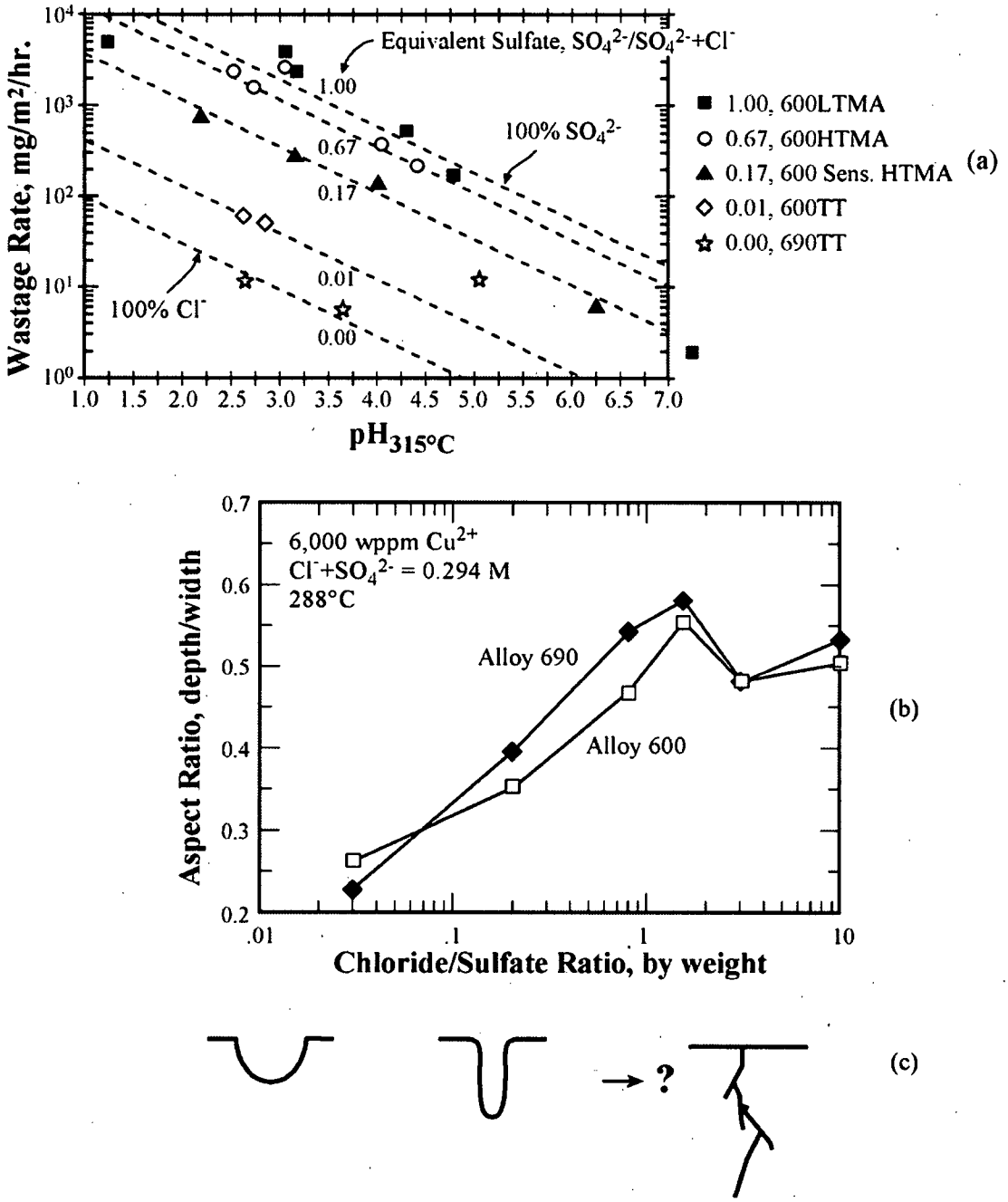


**Figure B.15.26** (a) Wastage rate vs. pH for retort tests using Alloys 600 and 690 in various heat treatments in concentrated acidified sulfate and chloride solutions at a test temperature of 315°C. Arrows point to top and bottom dotted lines corresponding to 100% sulfate and 100% chloride solutions. Column of numbers in the middle corresponds to the ratio of equivalent sulfate as $SO_4^{2-}/(SO_4^{2-} + Cl^-)$; value of 1.0 is all $SO_4^{2-}$ and value of 0.0 is all $Cl^-$. From Cullen.[34] © NACE International 1996. (b) Aspect ratio for pits vs. $Cl^-/SO_4^{2-}$ ratio for Alloys 600 and 690 exposed in 6000 wppm $Cu^{2+}$ at 288°C for $Cl^-+SO_4^{2-}$ = 0.294M. From Choi and Was.[35] © NACE International 1990. (c) Schematic view of implications of increasing acuity. From Staehle.[36] © NACE International 1996.

### 4.3 Near-Surface Environment Domain

A schematic view of the Near-Surface Environment Domain is shown in Figure B.15.18 as a part of the overall array of domains in Figure B.15.5. Examples from this domain are the following:

Heat transfer crevice

While the heat transfer crevice has been changed in the new generation of SGs, from the comprehensive envelopment of drilled holes, the occurrence of conditions for concentrating impurities persists as deposits continue to accumulate in line-contact geometries, although the resulting concentrations of species in these geometries have not been studied. Figures B.15.27a, b, c[37] show the nature of the chemical crevice in its complexity of chemistry, phases and gradients. Figures B.15.27d and e[1] show a schematic view of accumulation of deposits at egg crate line-contact crevices. These near-surface environments are substantially different from bulk environments in concentrations as well as in ratios of elements. Further, their chemistry changes in time. Such concentrating capacities of these crevices enable concentrating Pb, (e.g. from the ppt range to the low percentage range), at the metal-environment surfaces. It is likely that the line-contact accumulations will produce different chemistries from the drilled holes in view of the differences of geometry as these affect the concentration of species.

Accumulation of deposits and cells

Deposits accumulate with time due to superheat at the surfaces of tubes at tube supports and at the top of the tubesheet, as shown in Figures B.15.28a, b, c.[1] Such accumulations vary with locations. These deposits lead to the formation of electrochemical cells.

Deposit expansion and forces

Aside from the chemical and electrochemical aspects of deposits, as well as their heat transfer resistance; deposits also produce large forces in constrained geometries. Figure B.15.29, from the work of Pickering et al.,[23] shows a stainless steel specimen that was exposed in the non-stressed conditions with a stainless steel insert. The corrosion products that accumulated in the crevice between the specimen and the insert produced stresses, which caused SCC to start at the bottom of the crevice. After this SCC had propagated some distance, the insert was removed as part of the experimental program, and the corrosion products in the propagating SCC exerted sufficient force to cause the SCC to continue. These forces are produced by the larger specific volume of the oxide compared with the metal as reported in 1923 by Pilling and Bedworth.[24]

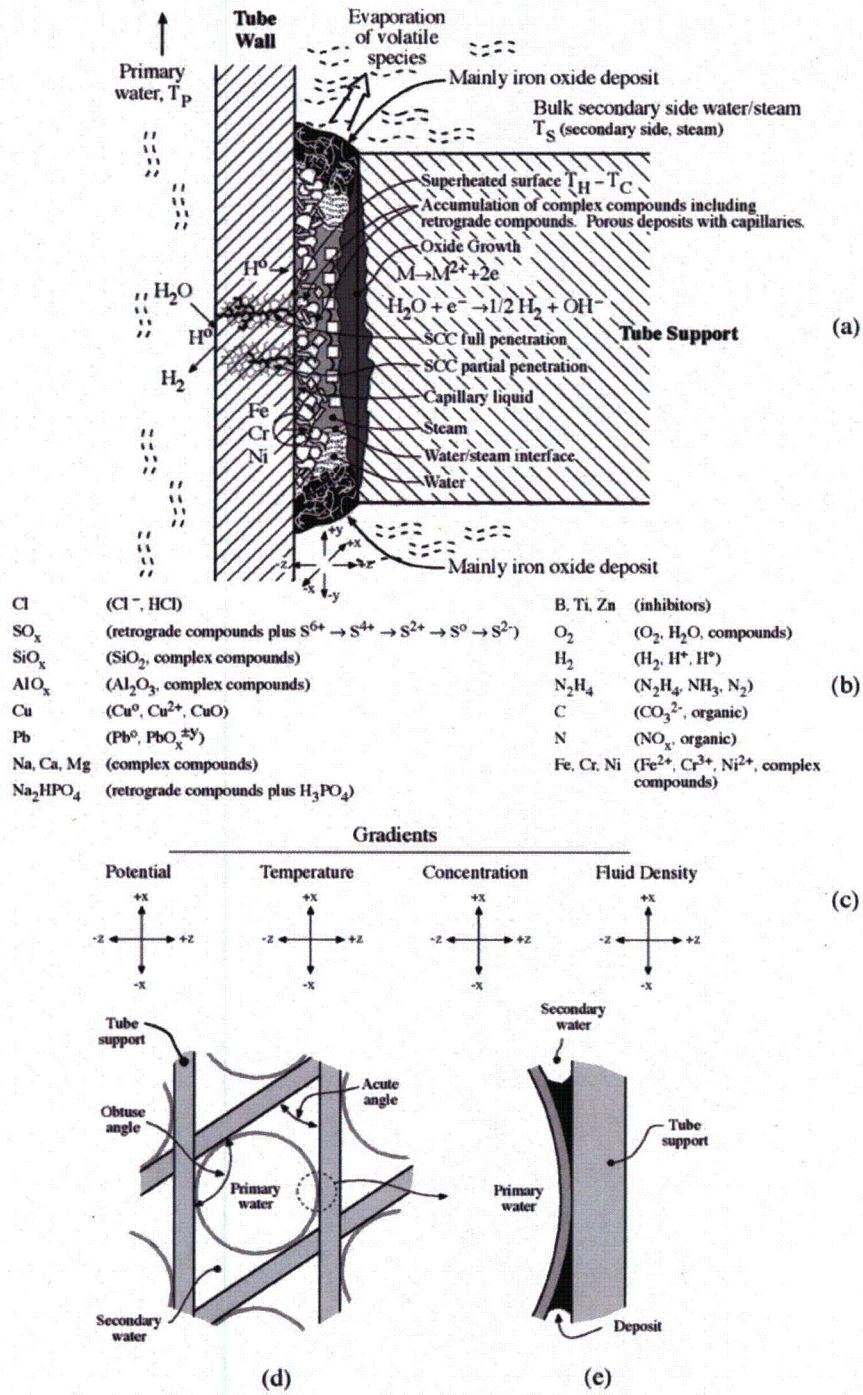


**Figure B.15.27** Schematic view of heat transfer crevice at a tube support. (a) Geometry. (b) Chemicals that accumulate and transform. (c) Types of gradients inside the heat transfer crevice. From Staehle.[37] (d) Egg crate design of tube support and (e) schematic view of accumulation of deposits in line-contact geometry, based on direct observations. From Staehle and Gorman.[1] © NACE International 2003/2004.

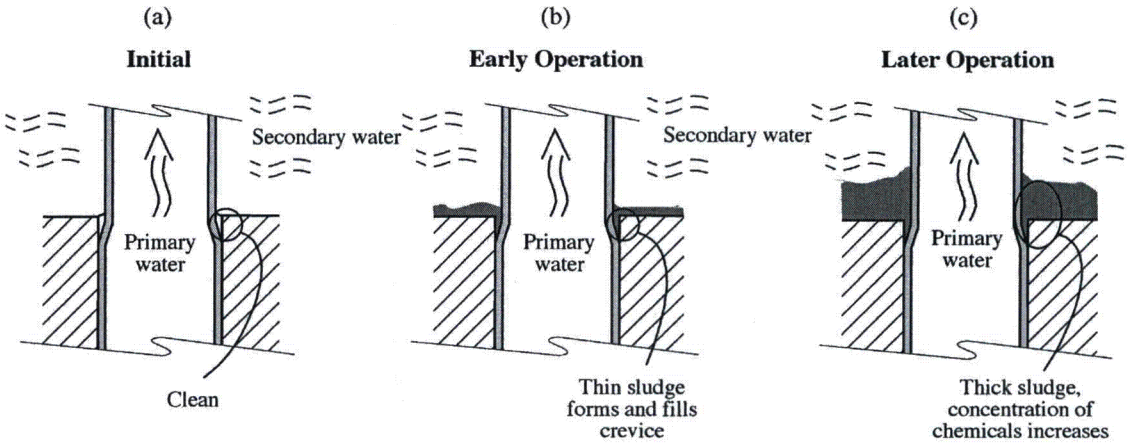


**Figure B.15.28** Accumulation of deposits on top of the tubesheet with time. From Staehle and Gorman.[1] © NACE International 2003/2004.

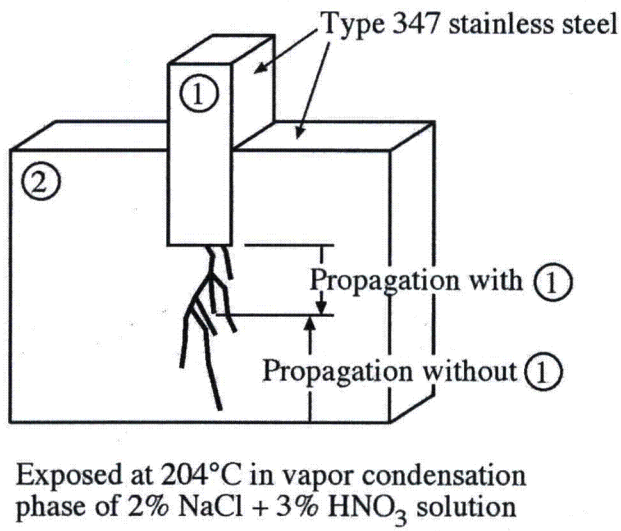


**Figure B.15.29** Demonstration of forces produced by corrosion products. Stainless steel block and insert exposed at 204°C in vapor condensation of 2% NaCl+3%$HNO_3$ solution; no applied stress. SCC propagates with corrosion product forces between block and insert. Insert removed and cracks propagate due only to corrosion products in initial cracks. From Pickering et al.[23]

### 4.4 Protective Film Domain

Properties of protective films dominate much of the corrosion behavior of metals. Further, this film interacts with slip processes in the metal and through its normal epitaxial connection to the metal, produces stresses in the substrate. Also, the defect concentration in the film catalytically affects oxidation and reduction reactions. The relative position of the protective film in the domains is shown in Figure B.15.5, and examples of important related microprocesses are shown in Figure B.15.19.

Epitaxial film growth

Epitaxial protective films grow with time according to various rate laws and following influences of alloy, pH, and potential. Figure B.15.30[38] shows the effect of potential and alloy composition on the thickness of protective films on iron base alloys. These films affect the catalytic influence on electrochemical reactions and the overall rate at which the alloy dissolves, as it is controlled by the properties of these films.

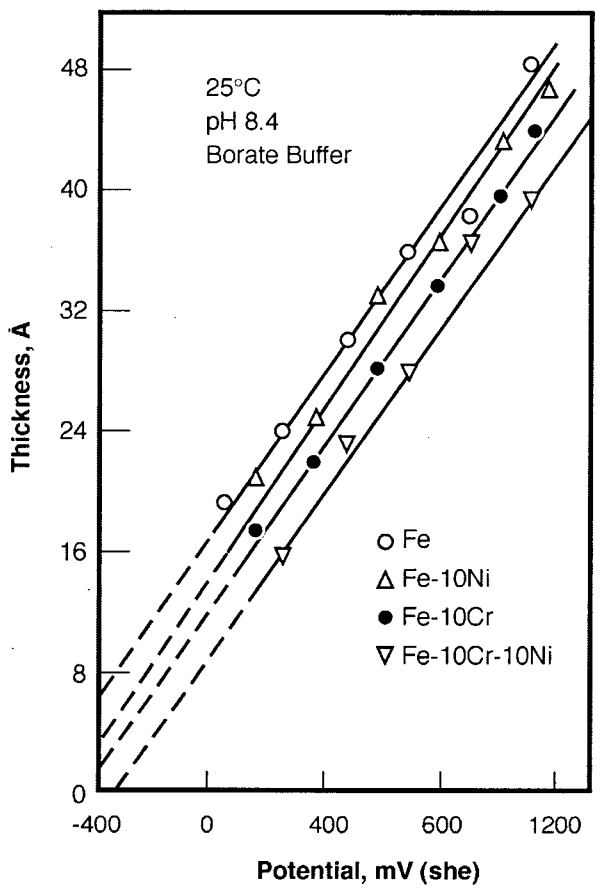


**Figure B.15.30** Film thickness vs. electrochemical potential for Fe, Fe-10Ni, Fe-10Cr, and Fe-10Ni-10Cr alloys after one hour of polarization at 25°C measured in a pH 8.4 borate buffer solution. From Goswami and Staehle.[38] Reprinted with permission from Elsevier.

Slip as affected by protective films

Figure B.15.31[39] shows the effect of epitaxial films on the single slip of a nickel single crystal. The protective film increases the work hardening, therefore increasing the slope, on the surface as shown by the work of Latanision and Staehle; whereas, the absence of the protective film permits the non-inhibited single slip. In the former, the slip steps are dispersed and finely divided; whereas, for the non-filmed surface, the slip is coarse and sharp. The presence of such films, then, affects the mechanical properties.

Brittle film rupture

Figure B.15.32[40,43] illustrates the process by which SCC proceeds as related to the formation of a brittle reaction product on the surface. Such a brittle surface might develop from the formation of an epitaxial reaction product such as is assumed for copper alloys in ammoniacal solutions. The periodic breaking of such a brittle film has been often suggested as the means of propagation of some SCC. The rate of crack propagation, then, is related to the growth rate of the brittle film.

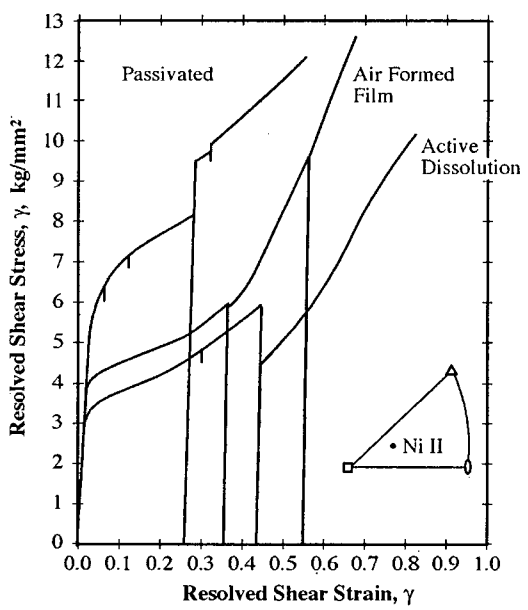


**Figure B.15.31** Flow curves illustrating the effect of interruptions in tensile tests under active and passive conditions. About 3-4 $\mu$m were removed from the crystal surface before deformation under dissolution conditions at a steady state current density of approximately 4 mA/cm$^2$. From Latanision and Staehle.[39] Reprinted with permission from Elsevier.

## 4.5 Near-Surface Metal Domain

Enrichment and depletion

As some alloys dissolve, the atoms may dissolve as "alloy atoms," so that they appear to be essentially the same atom, although of different chemistries.[41] Alternatively, in an alloy, especially where one atom is more electrochemically active than the other, (e.g. Cr in a Ni base or Zn in a Cu base), preferential loss of the more active Cr or Zn is expected, especially in the ranges of pH where the active species are also relatively soluble and in ranges of potential above the solution potentials for the more active species. Figure B.15.33a[41] shows data from Staehle based on work of Rockel; and Figure B.15.33b[42] shows data from Lumsden and Stocker. Figure B.15.33 shows that the surfaces of materials change with time from the original composition of the alloy due to the loss of Cr. Such a change affects the electrochemistry and the mechanical properties of the surface. These depletions and enrichments change the chemical composition of the surface, and thereby change the catalytic and mechanical properties of the near surface—sometimes producing a brittle layer similar to the one described in connection with Figure B.15.32.

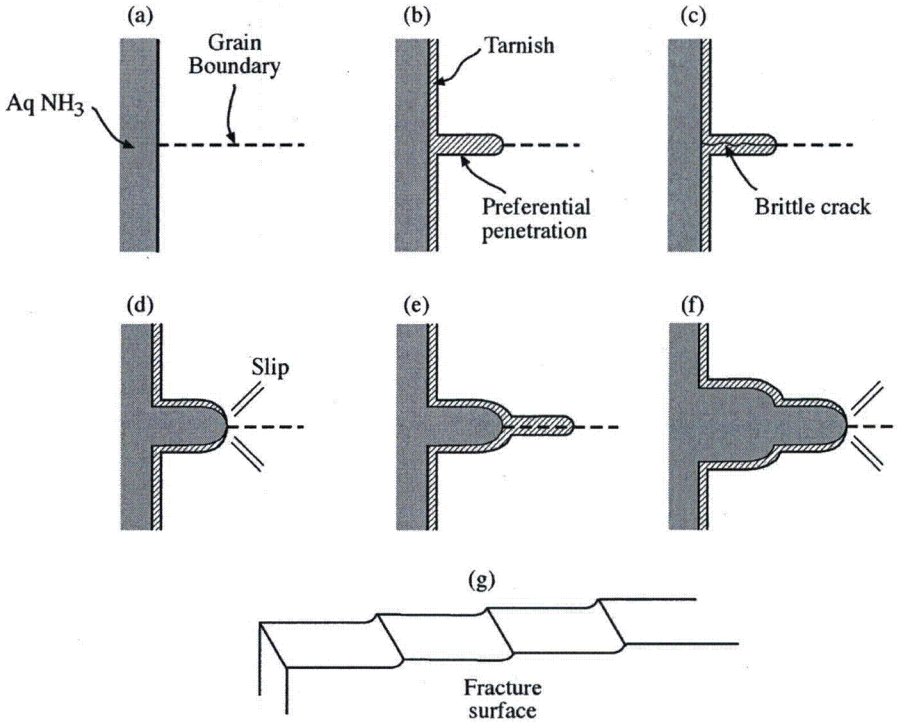


**Figure B.15.32** Formation of brittle film on surface followed by successive breaking thereby producing SCC. From Pugh et al.[40] © NACE International 1969 and Forty and Humble.[43]

Preferential dissolution of phases

In the same environment, the phases in a multiphase structure may dissolve differently. These differences depend on the pH and potential of the dominating environments. Figure B.15.34[44] shows that the relative dissolution of pearlite, $Fe_3C$ and α-Fe, depends on the pH and potential as well as species. Four modes of dissolution are observed: general dissolution independent of the phase, preferential dissolution of the α-Fe, preferential dissolution of the $Fe_3C$, and preferential dissolution of the interface between the $Fe_3C$ and α-Fe. Each of these modes could affect initiation and propagation of SCC.

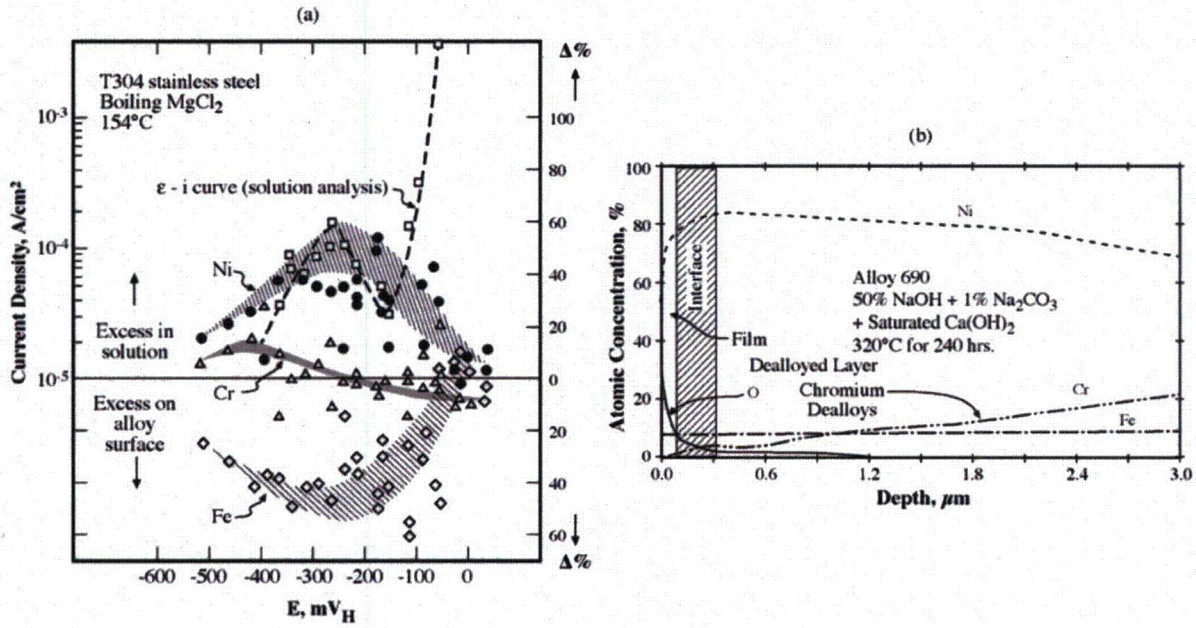


**Figure B.15.33** (a) Surface enrichment/impoverishment, Δ, of Fe, Cr and Ni on Type 304 steel in $MgCl_2$ at 154˚C as a function of applied potential. From Staehle.[41] © NATO-SCREC 1971. (b) Composition profile of Alloy 690 after exposure to 50% NaOH+1%$Na_2CO_3$+saturated $Ca(OH)_2$ at 320˚C for 240 h from depth analysis using Auger spectroscopy. From Lumsden and Stocker.[42] © NACE International 1988.

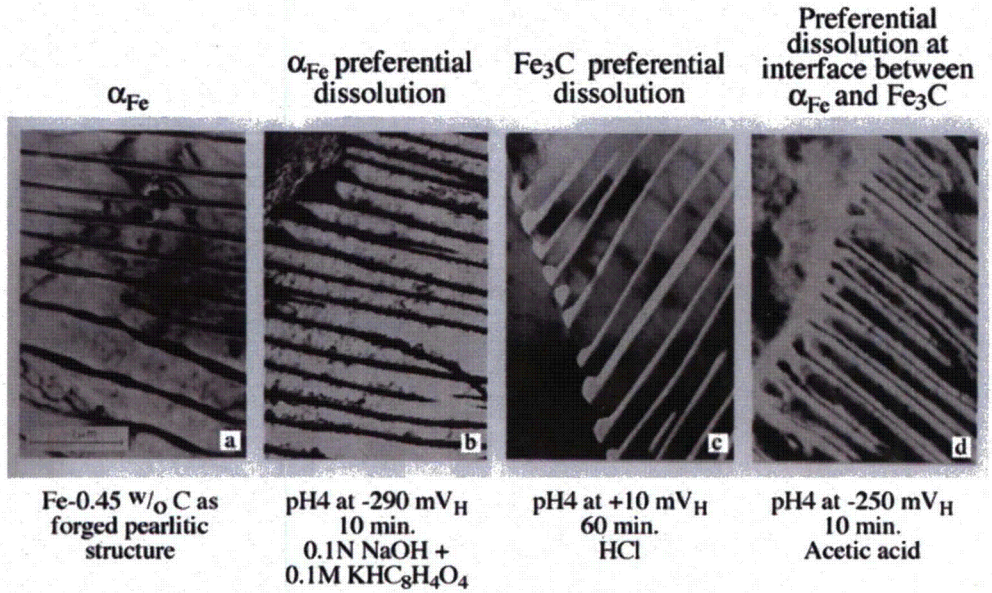


**Figure B.15.34** TEM micrographs of pearlite (1045 steel) foils exposed to various pH and potentials and species showing preferential dissolution of three types. From Payer and Staehle.[44] © NACE International 1974.

Slip trenches and tunnels

When dislocations move and intersect a passive surface, the passive film is broken; a transient dissolution event occurs, the metal initially dissolves, and then repassivates. Such events are shown in Figure B.15.35a.[45,46] In Figure B.15.35a, a thin foil has been exposed to a corrosive environment and stressed, after which it was examined in a transmission electron microscope. The image shows that parallel dissolution events have occurred within a single grain and that dissolution has occurred on both sides of the foil as shown by parallel dissolution traces. In this case, such parallel dissolution traces occur on intersecting slip planes. Figure B.15.35b[47] shows, by examining an oxide film, which was removed from the surface, that tunnels can emanate from the slip trenches observed in Figure B.15.35a. Conditions that support the transient dissolution of Figure B.15.35 depend on pH, potential and species in the environment. It is likely that environments that support transgranular SCC also support both the trenches and the tunnels of Figure B.15.35.

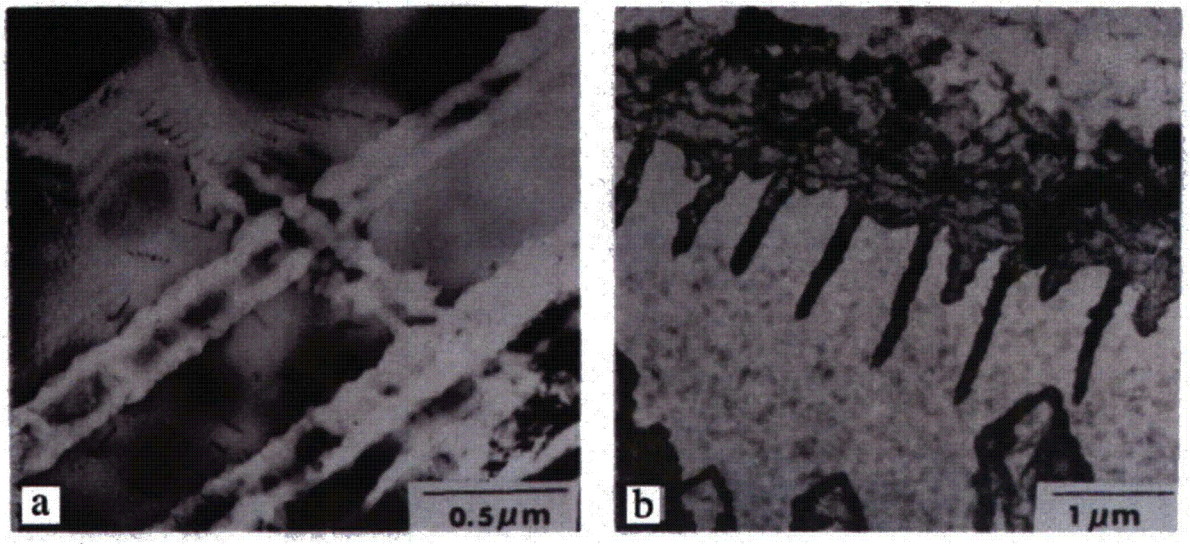


**Figure B.15.35** Two similar modes of corrosion at surfaces, which is associated with moving dislocations breaking the surface and protective film. (a) TEM image of thin Fe-Cr-Ni alloy foil stressed in a corrosive medium at RT and then examined in the TEM. Parallel thinned regions indicate preferential dissolution at both sides of the foil. Two slip systems are identified. From work of Smith[45] and Davis.[46] T.J. Smith, Master's Thesis at The Ohio State University 1965 and J.A. Davis, Ph.D. Dissertation at The Ohio State University 1968. (b) An oxide film removed from the surface of stainless steel after exposure in a stressed condition to a corrosive environment. The thick region corresponds to the slip dissolution trenches shown in (a) and the protrusions are "tunnels" that have penetrated from the base of the dissolution trench. From Long.[47] Master's Thesis, The Ohio State University, 1973.

## 4.6 Bulk metal domain

Stacking fault energy

Much of stress corrosion cracking and corrosion fatigue depend critically on the movement and relative coplanarity of movement of dislocations as they react to local stresses. There are two main patterns of dislocation movement that affect corrosion processes, as well as other aspects of deformation or fracture that are not considered here. Slip is important to SCC as it relates to breaking protective films, either during the slip process as shown in Figure B.15.35, or as the pile-up of dislocations at internal barriers intensifies local stresses at grain boundaries that interact with a corrosive environment.

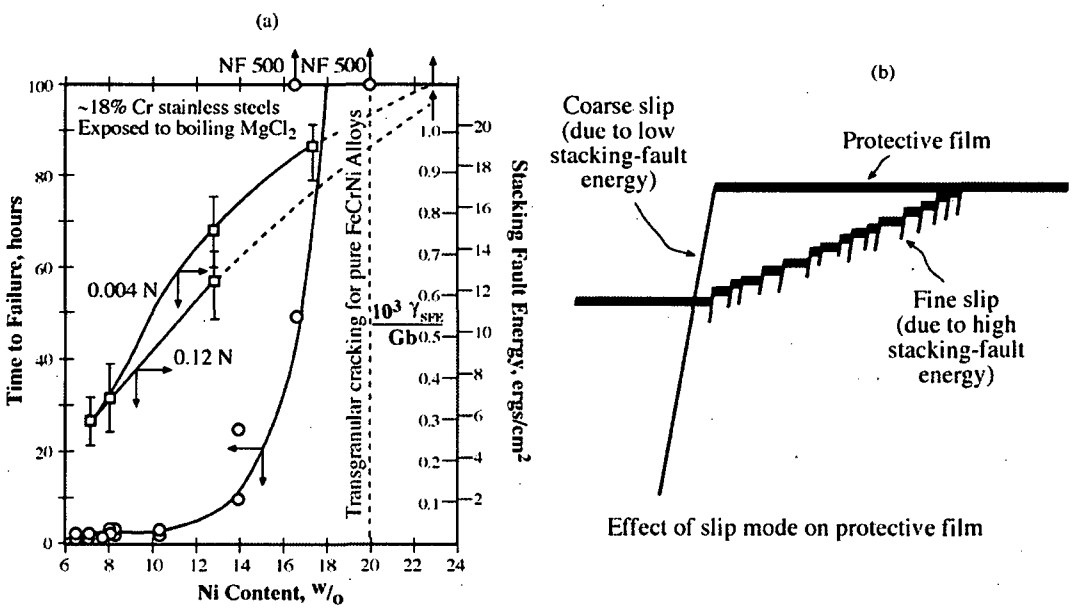


**Figure B.15.36** (a) Time-to-failure for 18%Cr stainless steels exposed to boiling $MgCl_2$ compared with stacking fault energies for the same materials. (b) Nature of slip as affected by relatively high and low stacking fault energies.

Both roles, single slip and cross slip, of dislocation movement are related to whether the slip remains generally on single slip planes to intensify local stresses and the sharpness of slip step at the surface or can cross slip to relieve the intensification of local stresses as well as producing distributed slip at the surfaces. Dislocations can be generally constrained to remain on single slip planes once nucleated. On the other hand, the dislocations might "cross slip" out of the single plane and thereby relieve the local pile-up stresses. These two tendencies depend on the "stacking fault energy." A high stacking fault energy stimulates cross slip, and a low stacking fault energy stimulates single slip. Thus, a high stacking fault energy would mitigate against SCC related to internal barriers; whereas, a low stacking fault energy would promote SCC. Figure B.15.36 shows how the stacking fault energy relates to SCC and to the nature of surface slip.

Composition of grain boundaries

The composition of grain boundaries is affected in two ways and according to somewhat different dimensional scales as shown in Figure B.15.37. Figure B.15.37a[7] refers to the formation of precipitates, such as chromium carbide, in stainless steel. The dimensions here are on the order of μm. Three conditions result from this process. First, the precipitate forms with a concentration of the metal typically greater than in the metal matrix. In the case of stainless steels, the compound is in the range of $Cr_{22}C_7$ or $Cr_7C_3$. This high concentration of chromium renders the alloy corrosion resistant in neutral solutions; but, in alkaline solutions the chromium is quite soluble relative to iron. Adjacent to the precipitate is a depleted zone from which the chromium has been taken to form the $Cr_xC_y$ compound. Such a zone, when depleted of chromium, is more prone to corrosion in neutral to acidic solutions but is more resistant to alkaline solutions. In addition, there is usually a narrow zone at the interface between the precipitate and the depleted zone where impurities are concentrated. Such interfaces have rarely been studied; but results, such as those in Figure B.15.34d, suggest that they could be prone to preferential corrosion depending on what species have been attracted or reflected during the formation of pearlite. Figure B.15.37c[7] shows the relative polarization rates for alloys across the range of alloy compositions.

In Figure B.15.37b,[7] the case of adsorption and desorption of species is shown for impurities and for alloying species. For the case of impurities, concentrations at the grain boundaries have been observed to be up to $10^6$ greater than in the grain matrix. The dimensions of these highly concentrated regions are in the range of nm. Such concentrations, although narrow, provide a reactive path for corrosion. Figure B.15.37d shows the effect of such adsorption on the cracking behavior of Ni with sulfur segregated at the grain boundary.[48,49]

Much of the preferential IGC and IGSCC is related to cases where such changes in concentration occur at grain boundaries as shown in Figure B.15.37.

## 5. Development of Scenarios

Developing a scenario is the essential process of predicting failures that occur after long times as shown in Figure B.15.1. A schematic illustration of developing a scenario is shown in Figure B.15.6. The scenario begins with the start of a power plant or from a suitable reference time, and identifies the components in the precursor as shown in Figure B.15.6. The components of the scenario are taken from the domains and their microprocesses, as described in Sections 3.0 and 4.0. Quantifying the microprocesses provides a basis for estimating the time before an SCC process can start. The times consumed by the developing microprocesses depend on the kinetic process that occur in the range of operating conditions of the plant. Further, it is likely that some of the microprocesses occur in sequence, thereby requiring the completion of one before the onset of the next. Finally, at the end of the precursor stage, the chemistry and configuration must lead to a viable SCC or other damage process.

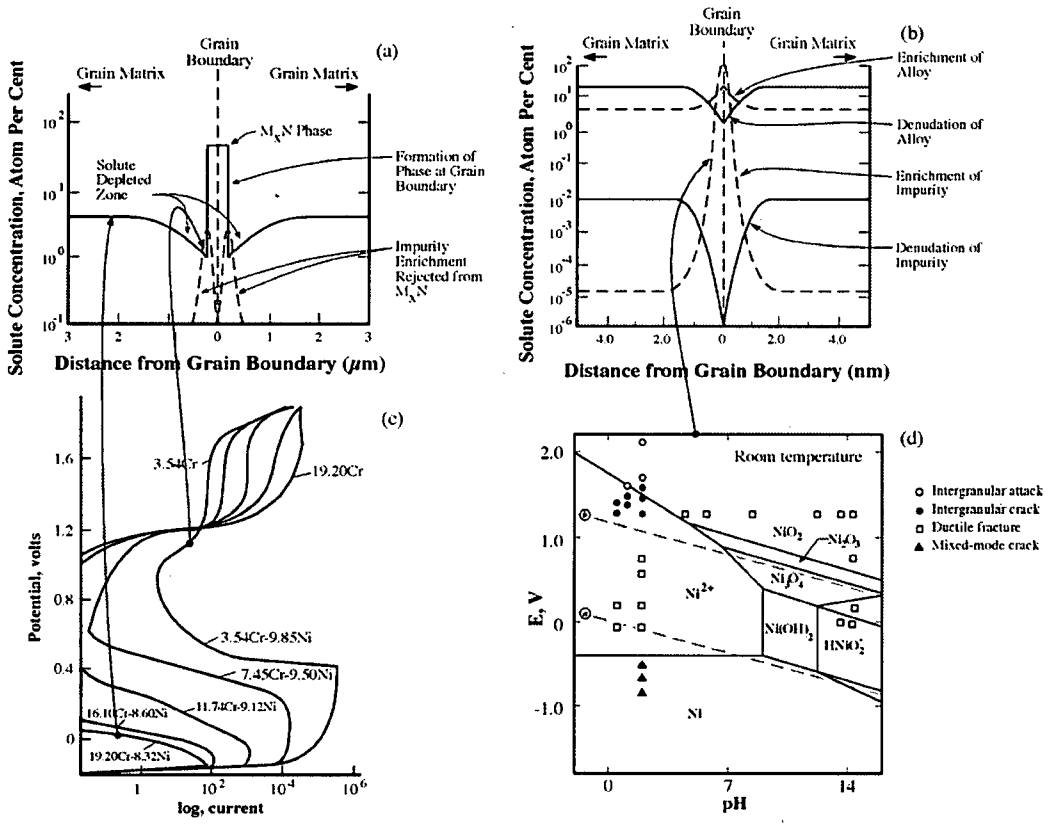


**Figure B.15.37** (a) Distribution of species at grain boundary for the case of precipitation. (b) Distribution for the case of adsorption. (c) Polarization behavior in sulfuric acid at RT for alloys across the grain boundaries. From Staehle.[7] Courtesy of John Wiley & Sons, New York. (d) Cracking behavior for a Ni-base alloy with sulfur segregation as a function of pH and potential. From Chaung et al.[48,49] Reprinted with permission from TMS.

Selecting the domains and microprocesses, as shown schematically in Figure B.15.6, requires expert experience. More than a single scenario would probably be considered.

Figure B.15.38 shows the overall process for selecting a scenario, evaluating the important rates upon which the length of the precursor stage is based, and applying the result to the starting point for the SCC.

## 6. Target

The goal of developing scenarios is to identify conditions under which SCC or some other important damage process will start according to the pattern of Figure B.15.1, Case III. For such a target to be achieved, the target itself needs to be identified. One might be LPSCC or PbSCC as shown in Figure B.15.22. However, there may be others. There is a task, then, of quantifying possible targets, which embody conditions initiating SCC, some of which have not occurred in the past but can reasonably be identified for possibly occurring in the future.

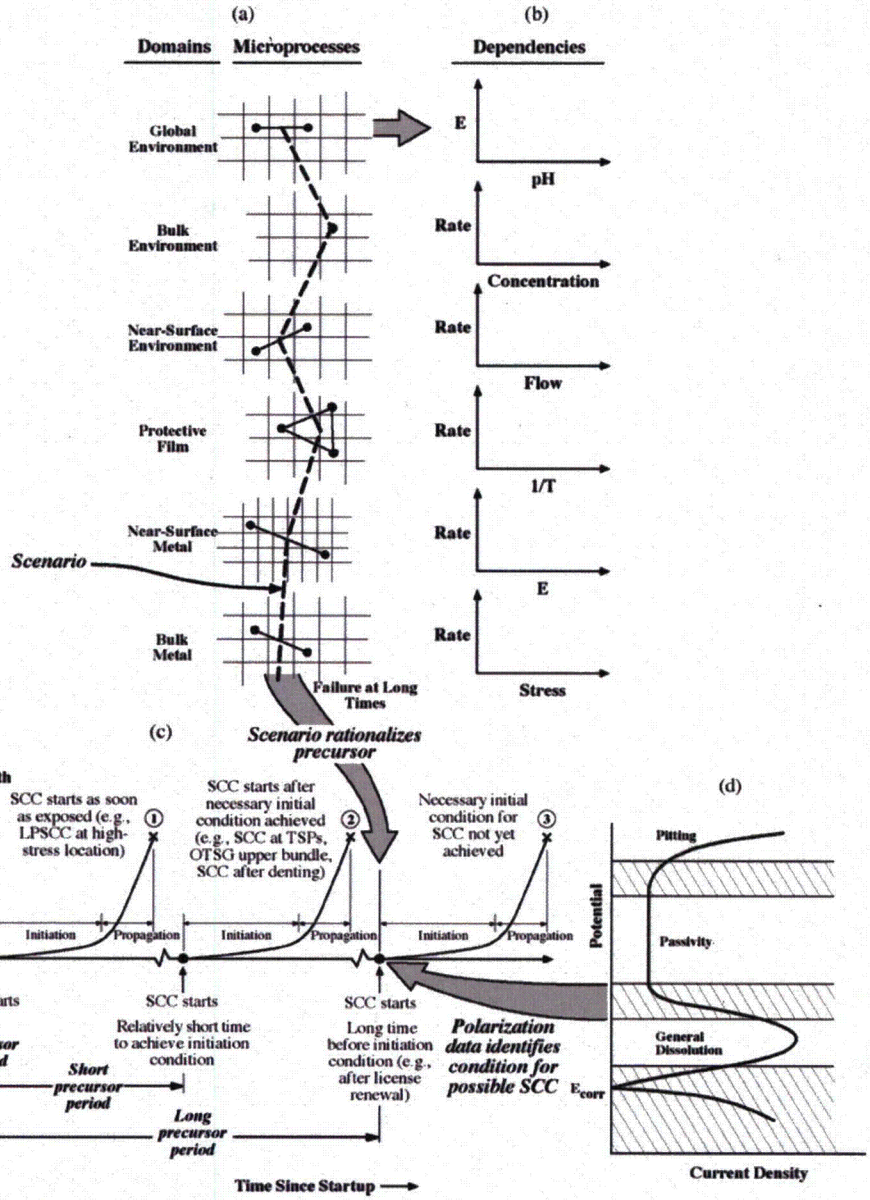


**Figure B.15.38** Schematic view of overall process of prediction. (a) Scenario including microprocesses from various domains; scenario connects microprocesses from various domains. (b) Hypothetical rates associated with microprocesses to be used for estimating length of precursor period. (c) Three cases for SCC with precursor times identified. (d) Possible location of target for SCC initiate.

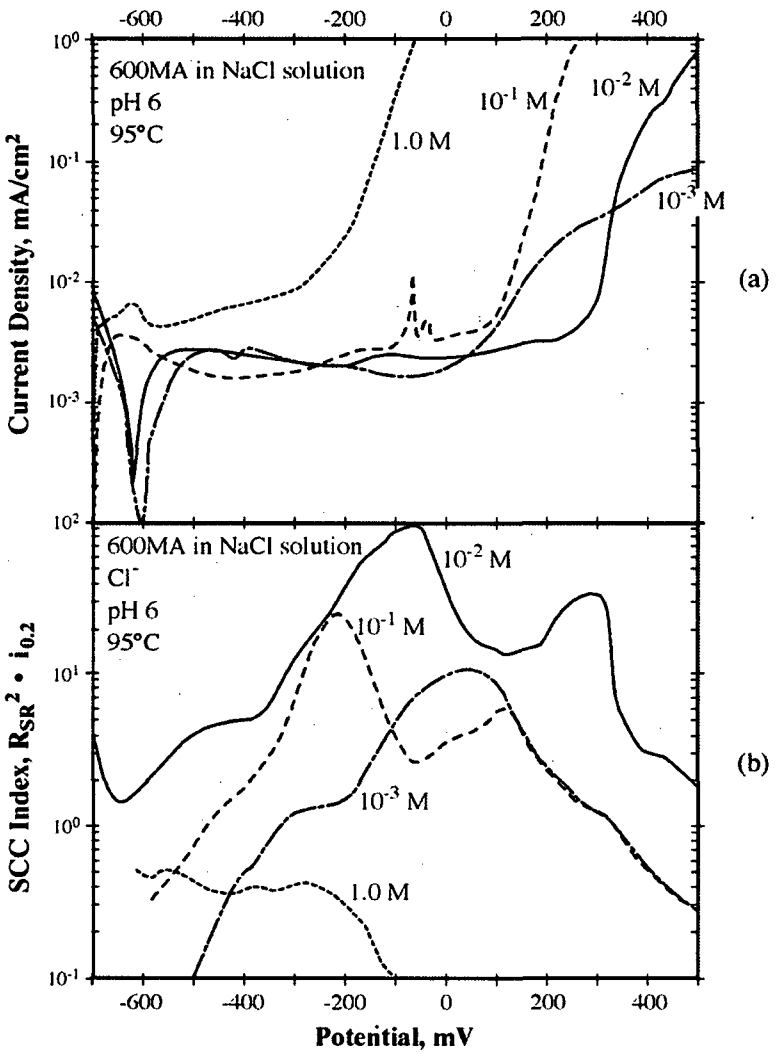


**Figure B.15.39** Current density and SCC parameter vs. potential for Alloy 600MA in NaCl solutions at pH 6 and 95°C for concentrations from $10^{-3}$ to 1.0 M. From Staehle and Fang.[50] Courtesy of SFEN.

Where some SCC is suspected to occur, but for which no information is available, there are several survey approaches that can be used and have been successful in the past. Figure B.15.39 suggests that locations for the initiation of SCC often occur at potentials near regions of kinetic instability. Such regions can be evaluated using electrochemical methods, either by identifying regions of transition such as in Figure B.15.38d, or regions where there are large differences between slow and fast scans. Figure B.15.39 shows polarization curves for Alloy 600MA in 95°C NaCl solutions. Figure B.15.39b shows a SCC parameter, which has been developed by Staehle and Fang[50] vs. potential. This parameter is based on the differences in currents between fast and slow potentiodynamic scans. Peaks in Figure B.15.39b identify potentials where SCC is likely.

Another approach for identifying regions of possible SCC has involved CERT tests that are conducted as functions of potential. Such data are shown in Figure B.15.40 from experiments by Parkins[51] and others.

There are other well-known methods for identifying targets of the scenarios suggested in Figures B.15.6 and B.15.38. The principal point here is that surveying possible future targets for scenarios is an important part of prediction. Such approaches can rely on the fact that the boundaries and domains of SCC are generally orderly, as suggested by Figure B.15.41, which shows the zone of SCC for stainless steel in acid chlorides at room temperature from the work of Morin and Staehle.[52,57]

## 7. Predictions

Using the approach described in Sections 3.0 and 4.0 and Figures B.15.1, B.15.6, and B.15.38 some predictions are possible, and examples of these are described in this section.

Transport of low valence sulfur to turbine

Figure B.15.42 shows a sequence of events involving the microprocesses described in Sections 3.0 and 4.0. The essence of prediction as shown in Figure B.15.42 is the following:

a. Sulfate impurities are reduced in steam generators by hydrazine to a low valence sulfur species (M-1) such as $HS^-$.

b. The low valence sulfur species is transported (M-2) to the turbine.

c. This low valence sulfur species deposits (M-3) on surfaces of the turbine where the materials are generally high strength alloys.

d. High strength alloys are prone to SCC and failure occurs after sufficient accumulation of the low valence sulfur species (M-4).

Such a possible sequence of events can be evaluated by:

a. Analyzing surfaces in turbines.

b. Evaluating the SCC behavior of turbine alloys in such environments as are found on surfaces.

LPSCC of Alloy 690 occurs as chromium is depleted from the surface

Figure B.15.43 shows a sequence of events whereby Alloy 690TT can sustain LPSCC as follows:

a. Chromium dissolves preferentially in the environment at moderately alkaline pH as shown in (M-1).

b. The surface, as it is depleted, (M-2), becomes an alloy like Alloy 600, as at (M-3), and sustains LPSCC as shown in (M-4).

This sequence implies that the LPSCC will propagate as rapidly as the chromium is depleted from the surface. This surface eventually becomes the crack tip; the tip of the crack then advances as rapidly as the chromium is preferentially dissolved. Such a possible sequence can be evaluated with ATEM and by evaluating the pH of solutions inside advancing SCC.

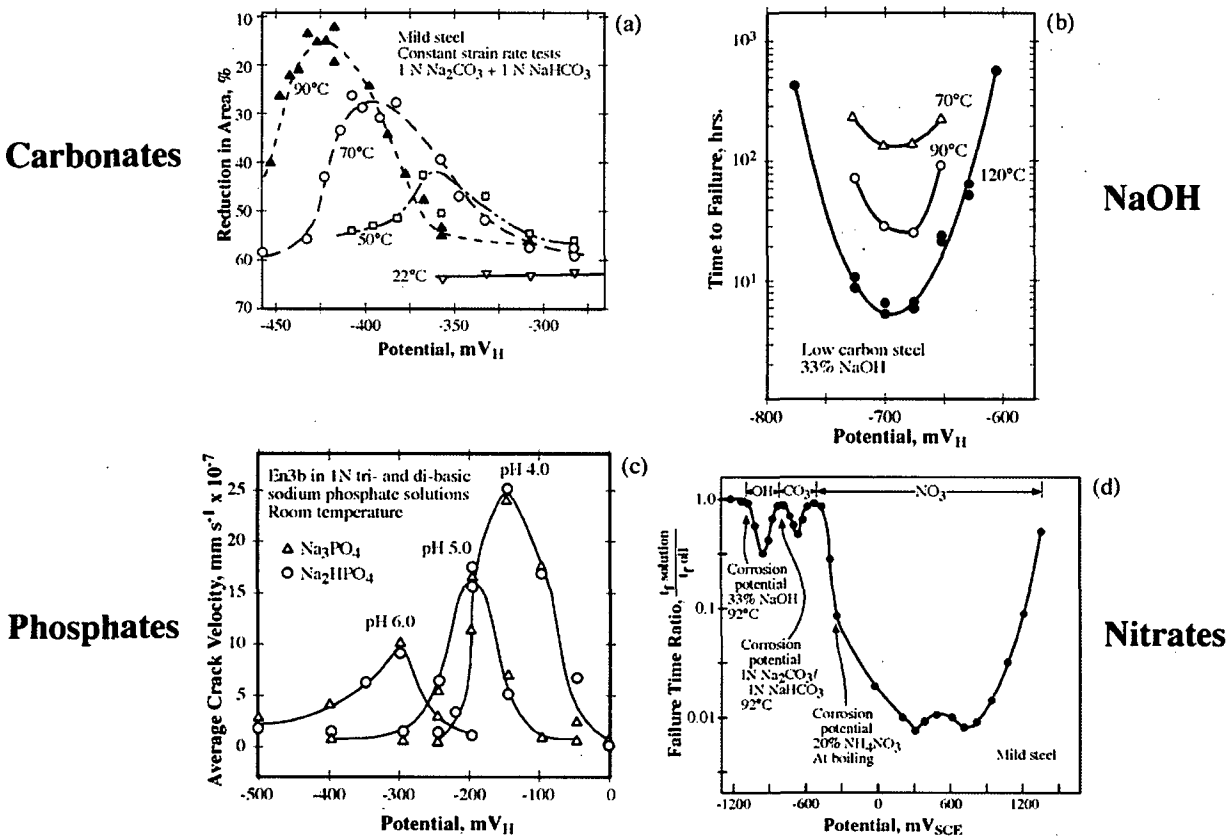


**Figure B.15.40** (a) Reduction in area vs. potential for mild steel exposed to carbonate-bicarbonate solutions at various temperatures and tested in CERT. From Sutcliffe et al.[53] © NACE International 1978. (b) Time-to-failure vs. potential for three temperatures for a low carbon steel in 33% NaOH. From Singh[54] (Courtesy of Steel India) reporting on Bohnenkamp.[55] © NACE International 1969. (c) Average crack velocities vs. potential for (plain carbon steel) En3b (w/o C 0.12, Si 0.05, Mn 0.81, S 0.029, P 0.008) steel in $Na_3PO_4$ and $Na_2HPO_4$ tested at RT function of pH. From Holroyd.[56] N.J.H. Holroyd PhD Dissertation 1977. (d) Ratio of time-to-failure in solution to time-to-failure in oil vs. potential for NaOH, $Na_2CO_3$ + $NaHCO_3$ and $NaNO_3$ solutions. From Parkins.[51] Courtesy of Inst. of Mat., Minerals & Mining 1972.

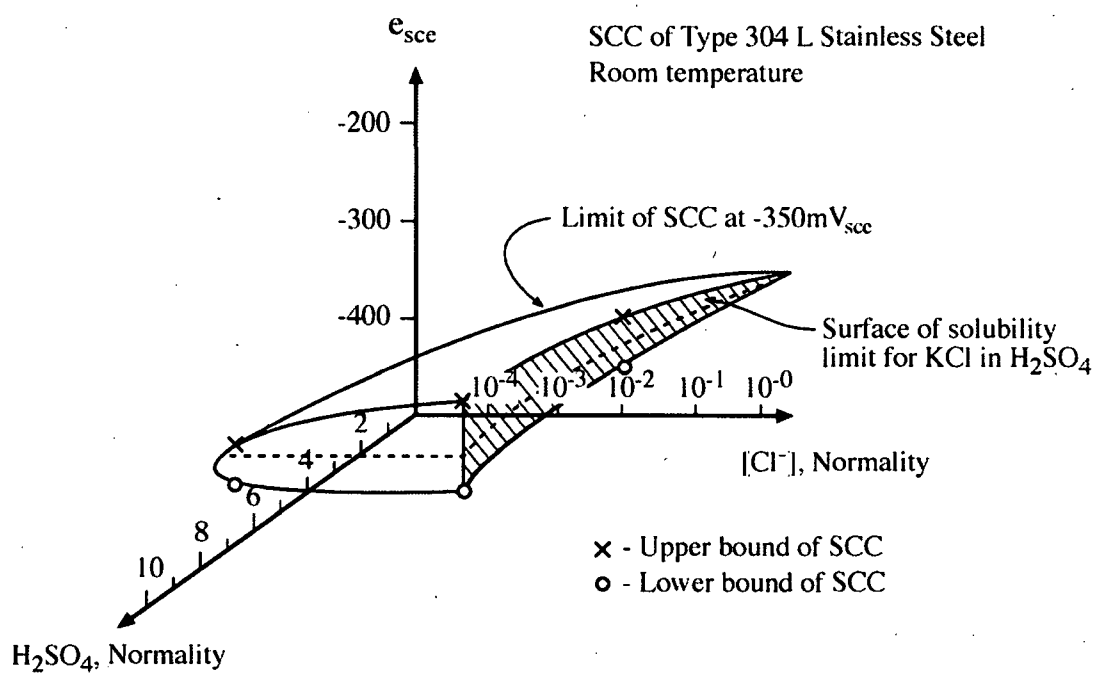


**Figure B.15.41** Zone for the occurrence of SCC in stainless steels as a function of potential, $H_2SO_4$, and KCl at room temperature. From Morin[57] C.R. Morin Master's Thesis, The Ohio State University 1972 and used by Staehle.[52] Reprinted with permission from TMS.

<u>PbSCC occurs as Pb is released from sequestering compounds</u>

One of the as yet unexplained observations in the performance of SGs is why massive PbSCC is not occurring despite the relatively large amount of Pb present in crevices and also known to be present in some stress corrosion cracks that have been examined. Further, Pb has been shown to produce SCC at relatively low concentrations of Pb. It also appears that PbSCC occurs readily in Alloy 690TT.

Thus, understanding why PbSCC does not occur when the threshold for concentration is so low and the PbSCC is so rapid, is an important question. The answer to why PbSCC does not occur seems related to the fact that the activity of Pb is lowered by the formation of Pb-containing compounds. Such compounds could include silicates, phosphates, sulfates, carbonates, or chlorides separately or as multiple component compounds.

Since the compounds that form in crevices are in some equilibrium with the species in the bulk water, reducing such species might raise the activity of the Pb making it available for producing PbSCC.

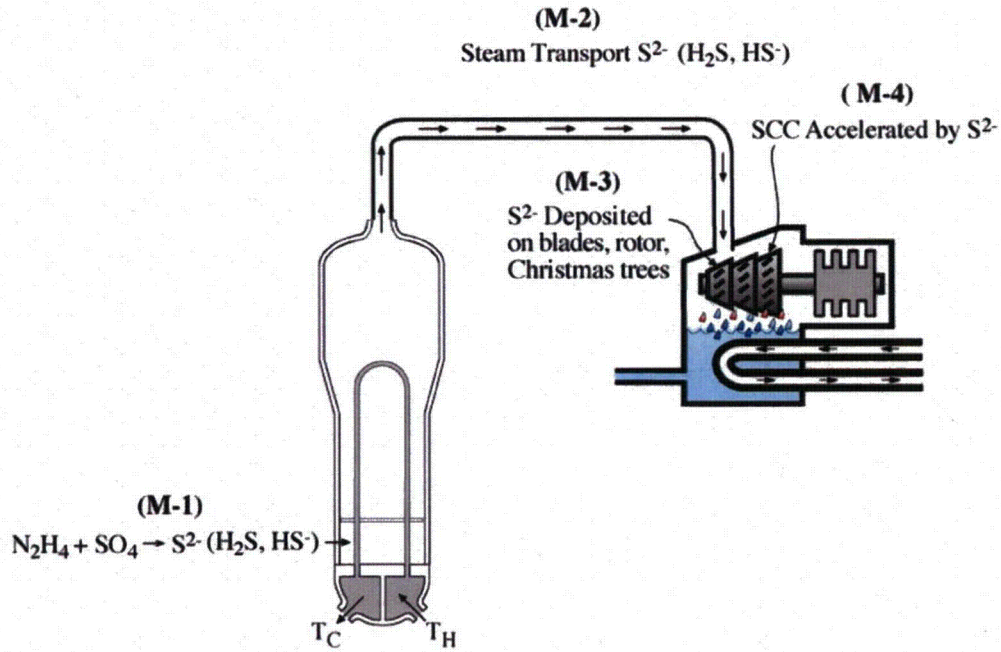


**Figure B.15.42** Reduction of $SO_4^{2-}$ by $N_2H_4$ in the SG and transport of reduced sulfur to the surfaces of the turbine where accelerated SCC is possible especially in view of high strength alloys from which the blades and rotors are constructed.

Figure B.15.44 shows a sequence of events associated with raising the activity of Pb by reducing the available compound-forming species.

a. Heat transfer crevices concentrate chemicals from feed water (M-1).

b. Lead enters heat transfer crevices (M-2).

c. A deposit forms containing Pb (M-3).

d. Pb concentrates on the hot surface as is observed from direct analysis (M-3).

e. Increasing the Pb activity is known to increase the intensity of PbSCC (M-4).

f. The activity of Pb will increase when the activity of compound forming species in the bulk water decreases (M-5).

Thus, it is possible that PbSCC will occur if the secondary water is further purified.

Such a process as described in Figure B.15.44 can be assessed by determining what compounds and chemical processes can immobilize the Pb. Such work has not yet been undertaken but it could predict the course of PbSCC.

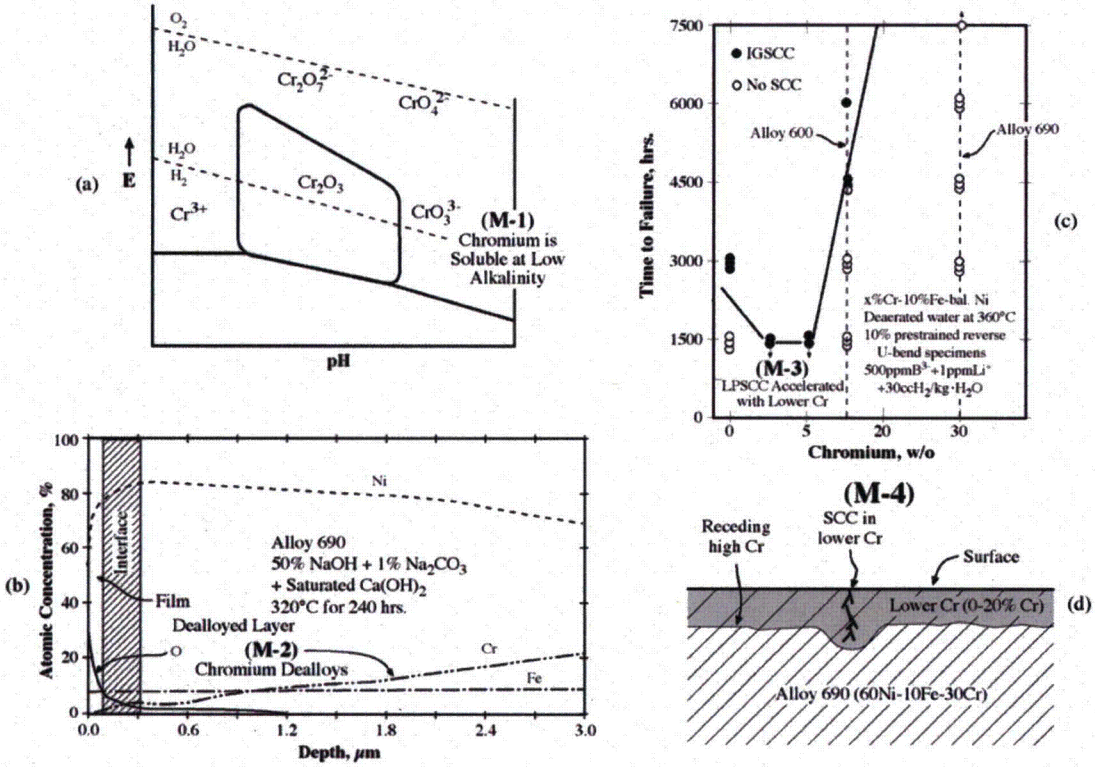


**Figure B.15.43** The Cr of Alloy 690 is soluble in mildly alkaline solution and dissolves to give a lower Cr surface and is more prone to LPSCC.

<u>SCC of low alloy steels in FAC type environments</u>

SCC is known to occur episodically in low alloy steels when exposed to FAC type environments as well as to other environments. The episodic nature of the SCC suggests that the high velocity of coolant is, in fact, removing the initiating events, and only initiating events whose velocities that exceed the recession rate of the FAC can actually become growing SCC. Such a pattern suggests that lowering the FAC rate may increase susceptibility to SCC according to the following sequence as shown in Figure B.15.45.

a. The rate of recession of a surface is greater than the rate of penetration of SCC initiation (M-1), (M-2).

b. The initial material is replaced with one having a lower rate of FAC; however, the rate of recession is less than the penetration rate during initiation. (M-3)

c. The rate of initiation now exceeds the rate of recession (M-4).

At this point SCC can initiate and propagate.

**(M-1) Concentration of Pb**

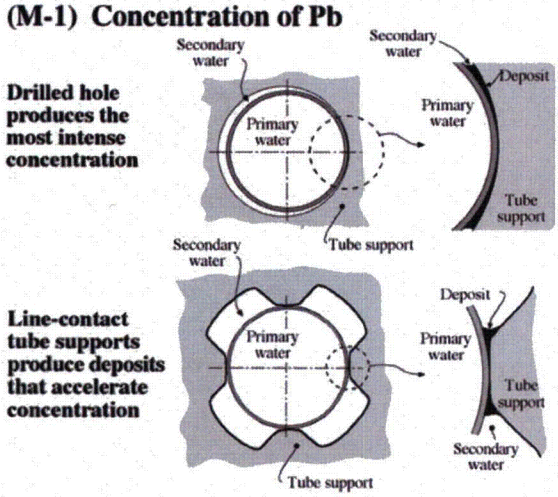


**(M-2)**

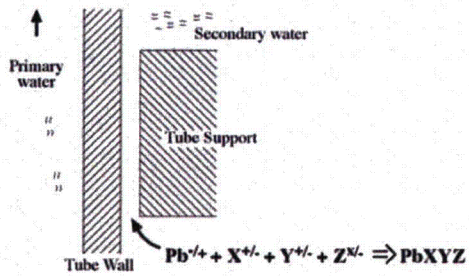


**(M-3)**

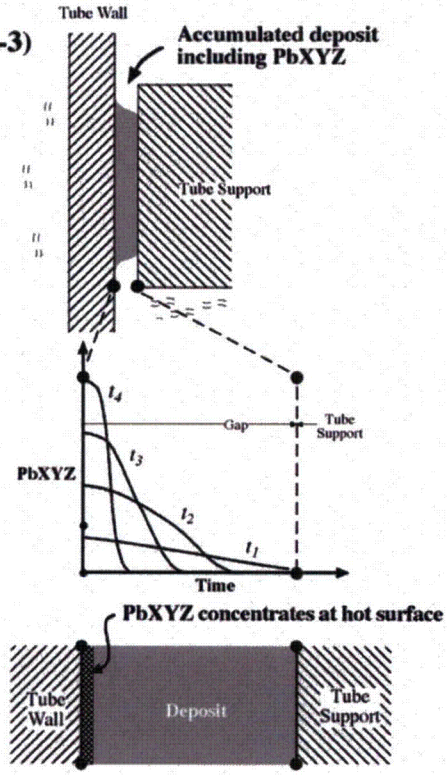


**(M-4)**

**PbSCC increases when Pb activity [$a_{Pb}$] increases at metal surface [$a_{Pb,\,s}$]**

1. **Pb activity increases when activity of compound-forming species decreases**

$$\text{e.g., } [a_{Pb,\,s}] \uparrow \text{ when } [a_{X,\,s}], [a_{Y,\,s}], [a_{Z,\,s}] \downarrow$$

2. **Activity of compound-forming species decreases on metal surface when these activities decrease in the bulk solution**

$$\text{e.g., } [a_{X,\,s}] \downarrow \text{ when } [a_{X,\,B}] \downarrow$$

**(M-5)**

**PbSCC increases when activity of compound-formers (X,Y,Z) decreases in bulk**

**Figure B.15.44** Pb is concentrated in heat transfer crevices and accumulates at the surface. Initially, Pb is immobilized by forming compounds. When the activity of these insolubilizing species is reduced, Pb is released and PbSCC occurs.

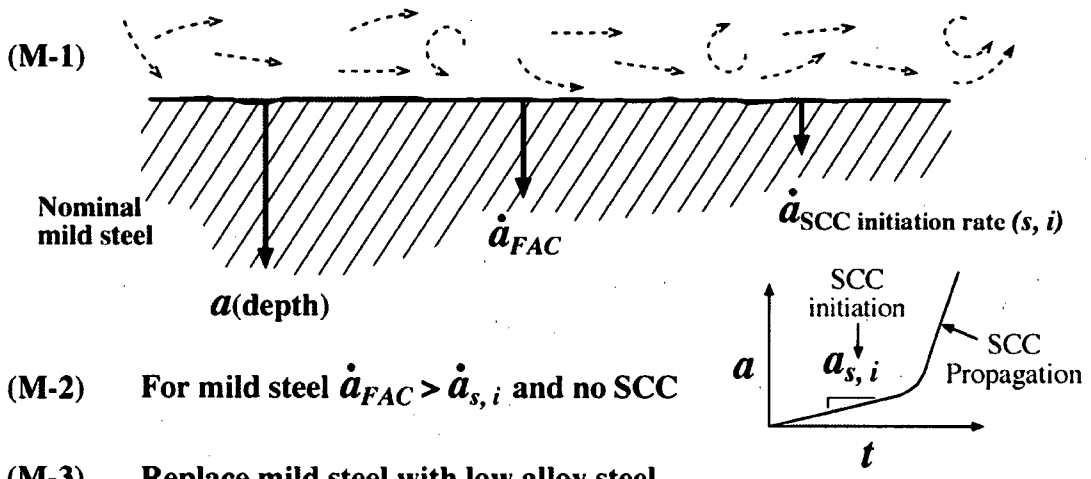


**(M-2)** **For mild steel $\dot{a}_{FAC} > \dot{a}_{s,\ i}$ and no SCC**

**(M-3)** **Replace mild steel with low alloy steel**

$$\dot{a}_{FAC}\ \text{(low alloy)} < \dot{a}_{FAC}\ \text{(mild steel)}$$

**(M-4)** $\dot{a}_{FAC}$ **(low alloy)** $< \dot{a}_{s,\ i}$

**(M-5)** **SCC initiates and propagates**

**Figure B.15.45** Sequence of events for reduction in rate of FAC and then permitting the SCC initiation process to accelerate and perforate.

## 8. Conclusions

1. In order to assure reliability for long time performance, methods for predicting corrosion failures that have not yet occurred should be considered. Such methods include the Microprocess Sequence Approach (MPSA).

2. The essence of predicting corrosion failures that occur after long times of service is recognizing that such processes as SCC will not proceed monotonically from the beginning of operation to a failure many tens of years later. Rather, predicting the occurrence of failures after long times most likely results from a multi-step analysis. First, there are some processes that develop conditions that are favorable to the later occurrence of SCC. The first steps are "precursors." Second, once the necessary conditions for SCC coalesce, then the SCC proceeds according to processes that produce failures in times between a month and ten years.

3. Thus, the long times which are necessary for failures to occur depend mainly on the times for precursors to develop.

4. Quantifying the precursor step can be approached by identifying microprocesses that require some time for maturing to produce the conditions necessary for SCC. In general, there might be multiple microprocesses acting in series or in parallel or both.

5. Organizing the microprocesses into a precursor stage is most effectively accomplished by recognizing that there are six domains that influence conditions for initiating SCC after some long time: global, bulk environment, near surface environment, protective film, near surface

metal, and bulk metal. Within each of these domains are microprocesses that are already known.

6. The quantitative development of a precursor scenario involves selecting a sequence of microprocesses that become logical constituents of a scenario. Multiple scenarios might be developed. Once such scenarios are identified, the time required for conditions to occur for SCC to initiate can be calculated. Such hypotheses can then be tested experimentally.

7. In addition to developing scenarios for precursors, it is necessary to identify what conditions must be met for SCC to occur. An array of such specific conditions can be assessed using various survey methods already well known.

8. The total time for failure to occur, then, involves the time for the precursor step to produce conditions necessary for SCC and the time for the SCC, once initiated, to propagate to failure.

## 9. Acknowledgements

The development of the ideas in this paper is based on many discussions with my colleagues in the corrosion community. Among these are Masatsune Akashi, Peter Andresen, Sam Armijo, Allen Baum, Ted Beck, John Bockris, Floyd Brown, Steve Bruemmer, H.E. Chaung, Pierre Combrade, John Congleton, Jacques Daret, Jim Davis, David Douglass, Zhi Fang, (the late) Mars Fontana, Bob Frankenthal, Rick Gangloff, Jack Gilman, Jeff Gorman, Mac Hall, John Hirth, (the late) Sam Hoar, Bill Hocking, Xiangchun Jiang, Rob Kelly, Jerry Kruger, Ronald Latanision, Bill Lindsay, Mike Long, Jesse Lumsden, Al McIlree, Charlie McMahon, Bruce Miglin, Peter Millett, Joe Muscara, Roger Newman, (the late) Peter Paine, (the late) Redvers Parkins, Joe Payer, Neal Pessall, Howard Pickering, (the late) Marcel Pourbaix, Neville Pugh, Bob Rapp, Peter Rhodes, Norio Sato, Steve Sawochka, Peter Scott, John C. Scully, John R. Scully, Masahiro Seo, Bill Shack, Toshio Shibata, Tetsuo Shoji, Karl Sieradski, Ed Simonen, Susan Smialowska, Tom Smith, Bill Smyrl, Markus Speidel, Narasi Sridhar, Norm Stoloff, Peter Swann, Bob Tapping, Larry Thomas, Gary Was, Jack Westbrook, Bert Westwood, Mike Wright, and many others.

I particularly appreciate the stimulation by Dr. Joe Muscara of the NRC to think about the subject in this report through his persistently advocating a proactive approach to predicting corrosion processes. I also appreciate the support of both Dr. Joe Muscara and Dr. Bill Shack of ANL for my research into predicting early SCC failures in steam generators.

I appreciate also the stimulating discussions of my colleagues in the PMDA group. Again, I thank Joe Muscara for bringing this project into being and for assembling such a group of outstanding colleagues.

Also, I greatly appreciate the careful reviews of this manuscript by Robert Tapping, William Shack, and Jack Westbrook.
Finally, as always, I thank my office staff who individually and as a group exhibit such high standards of professionalism in their attention to details and their refusal to compromise on lesser quality work. Specifically, I appreciate Julie Daugherty who prepared the manuscript in its final form and who resolved the many questions associated with sometimes inscrutable details; I also appreciate the talent and diligence that John Ilg brings to the preparation of my graphics. Marcia Parrish-Siggelkow and Erin Kate Rediger also assisted.

**References for B.15**


[1] R.W. Staehle , J.A. Gorman, "Quantitative Assessment of Submodes of Stress Corrosion Cracking on the Secondary Side of Steam Generator Tubing in Pressurized Water Reactors," Corrosion, Part 1 Vol. 59 No. 11 November 2003, Part 2 Vol. 60 No. 1 January 2004, Part 3 Vol. 60 No. 2, NACE, February 2004.

[2] D.O. Harris, E.Y. Lim, D.D. Dedhia, "Probability of pipe fracture in the primary coolant loop of a PWR plant," NUREG/CR-2189, Vol. 5, U.S. Nuclear Regulatory Commission, August 1981.

[3] D.O. Harris, D.D. Dedhia, S.C. Lu, "Theoretical and User's Manual for PC-PRAISE: A Probabilistic Fracture Mechanics Computer Code for Piping Reliability Analysis," NUREG/CR-5864, U.S. Nuclear Regulatory Commission, 1992.

[4] J.W. Provan, Probabilistic Fracture Mechanics and Reliability, Dordrecht, Boston, Massachusetts, 1987.

[5] T.L. Dickson, et al., "Pressurized Thermal Shock Probabilistic Fracture Mechanics Sensitivity Analysis for Yankee Rowe Reactor Pressure Vessel," NUREG/CR-5782, U.S. Nuclear Regulatory Commission, 2004.

[6] J.M. Bloom, J.C. Ekvall, Probabilistic Fracture Mechanics and Fatigue Methods: Applications for Structural Design and Maintenance – A Symposium, ASTM Committee E-9 on Fatigue; ASTM Committee E-24 on Fracture Testing, STP 798, American Society for Testing and Materials, Philadelphia, Pennsylvania, 1983.

[7] R.W. Staehle, "Lifetime Prediction of Materials in Environments," Uhlig's Corrosion Handbook, 2nd edition, pp. 27-84, Ed. R.W. Revie, John Wiley and Sons, New York, 2000.

[8] R.W. Staehle, "Approach to Predicting SCC on the Secondary Side of Steam Generators," presented at Fontevraud 5, Contribution of Materials Investigation to the Resolution of Problems Encountered in Pressurized Water Reactors, SFEN, Paris, September 23-27, 2002.

[9] R.W. Staehle, "Predicting the First Failure," presented at Corrosion 2003, San Diego, March 16-20, NACE, Houston, Texas, 2003.

[10] R.T. Begley, A.W. Klein, R.E. Gold, "Investigation of ID Stress Corrosion Cracking in Field and Laboratory Programs," Contribution of Materials Investigation to the Resolution of Problems Encountered in PWR Plants: International Symposium, French Nuclear Energy Society, Paris, 1985.

[11] R.W. Staehle, et al., "Application of Statistical Distributions to Characterizing and Predicting Corrosion of Tubing in Steam Generators of Pressurized Water Reactors" Life Prediction of Corrodible Structures, R.N. Parkins, ed., NACE, Houston, 1994.

[12] Private communication courtesy of R. Eaker of Duke Power, Charlotte, North Carolina.

[13] G. P. Airey, Optimization of Metallurgical Variables to Improve Corrosion Resistance on Inconel Alloy 600, EPRI NP-3051, Electric Power Research Institute, 1983.

[14] M.O. Speidel, R. Magdowski, "Stress Corrosion Crack Growth of Cold Worked Nickel Base Alloy 600," International Conference on Corrosion-Deformation Interactions; CDI '92, p. 107, Electricite de France, Paris, 1992.

[15] C.H. Shen, P.G. Shewmon, "A Mechanism for Hydrogen-Induced Intergranular Stress Corrosion Cracking in Alloy 600," Metallurgical Transactions Vol. 21A, p. 1261,1990.

[16] H.M. Chung, "Formation of Microcavities in BWR Core Shroud Welds," Proceedings of the Tenth International Conference on Environmental Degradation of Materials in Nuclear Power Systems – Water Reactors, P. Ford, G. Was, L. Nelson, eds., NACE, 2002.

[17] A. Kimura, "Dependence of Susceptibility to IGSCC on the Location of HAZ of Welded SUS304 Core Shroud for BWR," Proceedings of the Tenth International Conference on Environmental Degradation of Materials in Nuclear Power Systems – Water Reactors, P. Ford, G. Was, L. Nelson, eds., NACE, 2002.

[18] J. Hickling, et al., "Characteristics of Crack Propagation Through SCC Under BWR Conditions in Stainless Steels Stabilized with Titanium or Niobium," Proceedings of the Ninth International Conference on Environmental Degradation of Materials in Nuclear Power Systems – Water Reactors, p. 299-308, S.M. Bruemmer, F.P. Ford, G.S. Was, eds., TMS, 1999.

[19] K. Matocha, J. Wozniak, "Stress Corrosion Cracking Initiation in Austenitic Stainless Steel in High Temperature Water," Proceedings of the Ninth International Conference on Environmental Degradation of Materials in Nuclear Power Systems – Water Reactors, S.M. Bruemmer, F.P. Ford, G.S. Was, eds.,TMS, Warrendale, Pennsylvania, 1999, p. 383-388.

[20] E.D. Eason , L.M. Shusto, Analysis of Cracking in Small Diameter BWR Piping, EPRI NP 4394, Electric Power Research Institute, Palo Alto, 1986.

[21] T.M. Angeliu, et al., "Intergranular Stress Corrosion Cracking of Unsensitized Stainless Steels in BWR Environments," Proceedings of the Ninth International Conference on Environmental Degradation of Materials in Nuclear Power Systems – Water Reactors, p. 567, S.M. Bruemmer, F.P. Ford, G.S. Was, eds., TMS, 1999.

[22] M.O. Speidel , R. Magdowski, "Stress Corrosion Cracking of Stabilized Austenitic Stainless Steels in Various Types of Nuclear Power Plants," Proceedings of the Ninth International Conference on Environmental Degradation of Materials in Nuclear Power Systems – Water Reactors, p. 567, S.M. Bruemmer, F.P. Ford, G.S. Was, eds., TMS, 1999.

[23] H.W. Pickering, F.H. Beck, M.G. Fontana, "Wedging Action of Solid Corrosion Product During Stress Corrosion of Austenitic Stainless Steels," *Corrosion, 18*, p. 230-239, NACE, 1962.

[24] N.B. Pilling, R.E. Bedworth, "The Oxidation of Metals at High Temperatures," *Metals V, 29*, p. 529-582, 1923.

[25] D.P. Rochester, "Laboratory Investigation of Free-Span Axial Corrosion in Oconee Nuclear Station's Once Through Steam Generators," Water Chemistry of Nuclear Reactor Systems 8, British Nuclear Energy Society, London, 2000.

[26] D.P. Rochester , R.W. Eaker, "Laboratory Examination Results from Oconee Nuclear Station Once Through Steam Generator Tubes," Proceedings of the Ninth International Conference on Environmental Degradation of Materials in Nuclear Power Systems - Water Reactors, p. 639, S.M. Bruemmer, F.P. Ford, G.S. Was, eds., TMS, 1999.

[27] F.A. Garner, L.R. Greenwood, D.L. Harrod, "Potential High Fluence Response of Pressure Vessel Internals Constructed from Austenitic Stainless Steels," Proceedings of the Sixth International Conference on Environmental Degradation of Materials in Nuclear Power Systems – Water Reactors, R.E. Gold and E.P. Simonen, eds., TMS, 1993.

[28] S.M. Bruemmer, "New Issues Concerning Radiation-Induced Material Changes and Irradiation-Assisted Stress Corrosion Cracking in Light-Water Reactors," Proceedings of the Tenth International Conference on Environmental Degradation of Materials in Nuclear Power Systems – Water Reactors, P. Ford, G. Was, and L. Nelson, eds., NACE, 2002.

[29] J. Daret, et al., "Evidence for the Reduction of Sulfates under Representative SG Secondary Side Conditions, and for the Role of Reduced Sulfates on Alloy 600 Tubing Degradation," Proceedings of the Ninth International Conference on Environmental Degrada-

tion of Materials in Nuclear Power Systems – Water Reactors, p 567, S.M. Bruemmer, F.P. Ford, and G.S. Was, eds., TMS, 1999.

[30] T. Sakai, et al., "Effect of Reduced Sulfur on High Temperature Aqueous Corrosion for Alloy 600," Proceedings of the Fourth International Symposium on Environmental Degradation of Materials in Nuclear Power Systems - Water Reactors, p. 12/37, D. Cubicciotti, ed., NACE, 1990.

[31] B. Sala, et al., "Chemistry of Sulfur in High Temperature Water Reduction of Sulfates," Proceedings of the Fifth International Symposium on Environmental Degradation of Materials in Nuclear Power Systems - Water Reactors, American Nuclear Society, 1992.

[32] W.E. Allmon, P.L. Daniel, S.J. Potterton, "Conditions for the Chemical Reduction of Sulfates in an Aqueous Environment," Proceedings: Workshop on the Role of Sulfur Species on the Secondary-Side Degradation of Alloy 600 and Related Alloys, p. 10/1, EPRI NP-6710-SD, U.E. Gustafsson, ed., Electric Power Research Institute, 1990.

[33] O. de Bouvier, et al., "Influence of High Reducing Conditions on IGA/SCC of Alloy 600 in Neutral Sulfate Environments," 11th International Conference on Environmental Degradation of Materials in Nuclear Power Systems – Water Reactors, Stevenson, Washington, August 1-14, 2003.

[34] W.H. Cullen, "Review of IGA, IGSCC and Wastage of Alloys 600 and 690 in High Temperature Acidified Solutions," Control of Corrosion on the Secondary Side of Steam Generators, p. 273, R.W. Staehle, J.A. Gorman, and A.R. McIlree, eds. NACE, 1996.

[35] D. Choi, G.S. Was, "Pit Growth in Alloy 600/690 Steam Generator Tubes in Simulated Concentrated Environments (Cu2+, Cl- and SO42-)," *Corrosion, 46*, p. 100, 1990.

[36] R.W. Staehle, "Occurrence of Modes and Submodes of SCC," Control of Corrosion on the Secondary Side of Steam Generators, p. 135, R.W. Staehle, J.A. Gorman, and A.R. McIlree, eds., NACE, 1996.

[37] R.W. Staehle, "Bases for Predicting the Earliest Penetrations Due to SCC for Alloy 600 on the Secondary Side of PWR Steam Generators," NUREG-CR-6737, U.S. Nuclear Regulatory Commission, 2001.

[38] F.N. Goswami, R.W. Staehle, "Growth Kinetics of Passive Films on Fe, Fe-Ni, Fe-Cr, Fe-Cr-Ni Alloys, *Electrochimica Acta 16*, pp. 1895-1907, 1971.

[39] R.M. Latanision, R.W. Staehle, "Plastic Deformation of Electrochemically Polarized Nickel Single Crystals," *Acta Metallurgica, 17*, pp. 307-319, March, 1969.

[40] E.N. Pugh, J.V. Craig, A.J. Sedriks, "The Stress-Corrosion Cracking of Copper, Silver, and Gold Alloys," Proceedings of Conference Fundamental Aspects of Stress Corrosion Cracking, p. 118, NACE-1, September 11-15, 1967.

[41] R.W. Staehle, "Stress Corrosion Cracking of the Fe-Cr-Ni Alloy System," NATO Science Committee Research Evaluation Conference, from The Theory of Stress Corrosion Cracking in Alloys, edited by J.C. Scully, 1971.

[42] J.B. Lumsden, P.J. Stocker, "Inhibition of IGA in Nickel Base Alloys in Caustic Solutions," Corrosion '88, Paper 252, NACE, March 21-25, 1988.

[43] A.J. Forty and P. Humble, *Phil.Mag., 8*, 247, 1963.

[44] J.H. Payer , R.W. Staehle, "Dissolution Behavior of Carbides in Aqueous Environments," Localized Corrosion, NACE-3, Eds. R.W. Staehle, B.F. Brown, J. Kurger and A. Agrawal, NACE, 1974, conference held at Williamsburg, Virginia, December 6-10, 1971.

[45] T. Smith, "Relationship of Defect Structure to the Corrosion Behavior of Some Austenitic Stainless Steels," M.S. Thesis, The Ohio State University, 1965.

[46] J.A. Davis, "Local Dissolution Phenomena Occurring on Iron-Chromium-Nickel Alloys: An Electron Microscopic Study," Ph.D. Dissertation, The Ohio State University, 1968.

[47] M. Long, "The Polarization Behavior of Iron-Nickel-Chromium Alloys in Caustic Solutions," M.S. Thesis, The Ohio State University, 1973.

[48] H.E. Chaung, Z. Szklarska-Smialowska, R.W. Staehle, "The Effects of Heat Treatment on Surface Segregation in Inconel 600," *Scripta Metallurgica, 13,* 1979.

[49] H.E. Chaung, J.B. Lumsden, R.W. Staehle, "Effect of Segregated Sulfur on the Stress Corrosion Susceptibility of Nickel," Metallurgical Transactions 10A, 1979.

[50] R.W. Staehle , Z. Fang, "SCC of Alloys 600 and 690 in the Mid-Range of pH," presented at the International Symposium Fontevraud IV, Contribution of Materials Investigation to the Resolution of Problems Encountered in Pressurized Water Reactors, September 14-18, 1998.

[51] R.N. Parkins, et al., "Stress Corrosion Test Methods," *British Corrosion Journal, 7*, p. 154, 1972.

[52] R.W. Staehle, "Development and Application of Corrosion Mode Diagrams," Parkins Symposium on Stress Corrosion Cracking, pp. 447-491, Eds. S.M. Bruemmer, E.I. Meletis, R.H. Jones, W.W. Gerberich, F.P. Ford, and R.W. Staehle, Cincinnati, Ohio, October 21-24, 1991, TMS (The Minerals, Metals and Materials Society), 1992.

[53] J.M. Sutcliffe, et al., "Stress Corrosion Cracking of Carbon Steel in Carbonate Solutions," *Corrosion, 28*, p. 313, 1978.

[54] V.K. Singh, "Stress Corrosion Cracking of Low-Carbon and Low-Alloy Steels," *Steel India, 11*, p. 53, 1988.

[55] K. Bohnenkamp, "Caustic Cracking of Mild Steel," Fundamental Aspects of Stress Corrosion Cracking, p. 374, NACE-1, R.W. Staehle, A.J. Forty, and D. van Rooyen, eds., NACE, 1969.

[56] N.J.H. Holroyd, "Environmental Aspects of Stress Corrosion Cracking of Ferritic Steels," Ph.D. Thesis, University of Newcastle-upon-Tyne, 1977.

[57] C.R. Morin, "Potential Dependent Stress Corrosion Cracking of Type 304-L Stainless Steel in H2SO4 + KCl at 25°C," Thesis presented in partial fulfillment of the requirement for degree of Master of Science, The Ohio State University, 1972.